Modeling and Analysis of Point-to-Multipoint Millimeter Wave Backhaul Networks

Jia Shi, *Member, IEEE*, Lu Lv, Qiang Ni, *Senior Member, IEEE*, Haris Pervaiz, *Member, IEEE*, and Claudio Paoloni, *Senior Member, IEEE*

***Abstract*— A tractable stochastic geometry model is proposed to characterize the performance of novel point-to-multipoint (P2MP) assisted backhaul networks with millimeter-wave (mm-wave) capability. The novel performance analysis is studied based on the general backhaul network (GBN) and the simplified backhaul network (SBN) models. To analyze the signal-to-interference-plus-noise ratio (SINR) coverage probability of the backhaul networks, a range of the exact- and closed-form expressions are derived for both the GBN and SBN models. With the aid of the tractable model, the optimal power control algorithm is proposed for maximizing the trade-off between energy-efficiency (EE) and area spectral-efficiency (ASE) for the mm-wave backhaul networks. The analytical results of the SINR coverage probability are validated, and they match those obtained from Monte-Carlo experiments. The numerical results of the ASE performance demonstrate the significant effectiveness of our P2MP architecture over the traditional point-to-point setup. Moreover, our P2MP mm-wave backhaul networks are able to achieve dramatically higher rate performance than that obtained by the ultra-high-frequency networks. Furthermore, to achieve optimal EE and ASE tradeoff, the mm-wave backhaul networks should be designed to limit the link distances and line-of-sight interferences while optimizing the transmission power.**

***Index Terms*— Millimeter wave wireless backhaul networks, point-to-multipoint.**

I. Introduction

OVER the past few years, global mobile traffic has an explosive rate increasing with 131% annual growth, and the peak data rate has increased with 55% annual growth [1]. However, low frequency bands, such as ultra high frequency (UHF), have been heavily utilized and it is difficult to find sufficient frequency bands in the sub 6 GHz range for 5G cellular networks. In comparison, there are still a large number of unused spectrum resources in the millimeter-wave (mm-wave) bands, which may be of potential exploiting to future networks. Therefore, employing mm-wave high frequency bands such as 30-300 GHz and network densification are considered as key enablers to achieve high requirements of data rate, energy efficiency and spectrum efficiency for future 5G wireless networks [2]–[8].

Manuscript received July 31, 2017; revised July 13, 2018; accepted October 17, 2018. Date of publication November 8, 2018; date of current version January 8, 2019. This work was supported in part by the EU H2020 TWEETHER Project under Grant 644678, in part by the National Natural Foundation of China under Grant 61631015, in part by the Royal Society Project under Grant IEC170324, and in part by EPSRC under Grant EP/P015883/1. The associate editor coordinating the review of this paper and approving it for publication was S. Pollin. *(Corresponding authors: Qiang Ni; Lu Lv.)*

J. Shi and L. Lv are with the State Key Laboratory of Integrated Services Networks, Xidian University, Xi'an 710071, China (e-mail: jiashi@xidian.edu.cn; lulv@stu.xidian.edu.cn).

Q. Ni and H. Pervaiz are with the School of Computing and Communications, Lancaster University, Lancaster LA1 4WA, U.K. (e-mail: q.ni@lancaster.ac.uk; h.b.pervaiz@lancaster.ac.uk).

C. Paoloni is with the Department of Engineering, Lancaster University, Lancaster LA1 4YW, U.K. (e-mail: c.paoloni@lancaster.ac.uk).

Color versions of one or more of the figures in this paper are available online at http://ieeexplore.ieee.org.

Digital Object Identifier 10.1109/TWC.2018.2879109

A. Related Works

Increasing research efforts have been carried out to investigate the potential of mm-wave cellular networks, such as easier deployment, superior rate coverage and higher throughput for indoor/outdoor environment [9]–[15]. Most of the work in the literature, such as [9]–[13], have mainly focused on utilizing mm-wave spectrum on access networks for future wireless communications. An initial theoretical study on the capacity and coverage of cellular networks using mm-wave frequency bands has been addressed in [11]. mm-wave cellular networks [12], [13] have been focused on the physical layer security issues by exploiting the benefit from using directional antennas. More recently, some research attentions [16], [17] have been devoted to the ultra dense hybrid heterogeneous cellular networks with both UHF and mm-wave BSs coexisting. As proposed by [17], mm-wave BSs only support downlink transmission whereas UHF BSs support both downlink and uplink transmissions. However, the above studies have revealed that high path loss and severe penetration loss due to physical blockages pose huge challenges to the implementation of mm-wave access networks, especially the physical limitations of realizing mm-wave terminals.

It is still very challenging to realize mm-wave communication in access networks due to the facts that, equipping high-cost mm-wave antennas at mobile users, and high signal overhead caused by beam training and tracking, as well as diverse interference scenario. These issues will be alleviated in backhaul networks, which certainly provide a better scenario for employing mm-wave than access networks. Nevertheless, very limited research efforts have been devoted to mm-wave backhaul networks. Recently, suggested by [18]–[20], mm-wave communication is considered as a key enabler for providing the wireless backhaul for outdoor small cells due to massive spectrum available providing high capacity, quick deployment, flexibility, and low cost in comparison to fibre. The studies

of [19] and [20] have proposed the optimal strategies for small-cell BS deployment in order to design high-efficient mm-wave backhaul networks. Furthermore, a range of researches in [14], [15] and [21] have focused on jointly designing the access and backhaul networks with mm-wave capability. References [14] and [15] have studied the HetNet with mm-wave communication for access and backhaul, and have investigated multihop routing schemes for the mm-wave-based backhaul mesh. Shariat *et al.* [21] have addressed the issue of managing radio resources for the access and backhaul links in the small cell networks. Apparently, the current researches have barely analyzed the theoretical performances of mm-wave backhaul networks, especially by means of stochastic geometry approach.

By exploiting a range of advantages, point-to-multipoint (P2MP) technique at mm-wave will open new perspective for future backhaul networks. On one hand, P2MP approach can increase link utilization thus achieving higher throughput, compared to traditional point-to-point (P2P). On the other hand, P2MP approach requires much lower hardware cost for a single link than the P2P approach. In the literatures, P2MP technique has been exploited by various mm-wave access networks, such as [22] and [23] investigated the P2MP assisted WLAN systems operating at 60 GHz. By contrast, the very limited studies [24]–[26] have been devoted to investigating P2MP technique assisted wireless backhaul networks. In [24], a TDM-based scheduling for in-band access and backhaul links has been investigated to support point-to-multipoint and non-LOS communication. Zhang *et al.* [25] have proposed a novel two-tier backhaul networks, where P2MP technique is applied to UHF-based links, while however using P2P technique for mm-wave-based links. Further, in [26], the engineering challenges have been addressed for implementing the Q-band backhaul link with P2MP.

B. Motivations and Contributions

So far, there is no satisfactory P2MP based backhaul solution in mm-wave, which is urgently desired by theoretical study and industry. In this trend, our EU funded TWEETHER project[1] is to set a milestone in the millimetre wave technology with the realization of the first W-band (92-95GHz) wireless system, supported by the high power of a new concept of traveling wave tube [27]. The long range achieved by the transmission hub proposes a credible solution for high capacity density and availability [28]. TWEETHER aims to realise the millimetre wave P2MP segment to link fibre, and sub-6 GHz distribution for a full three segment hybrid network, that is the most cost-effective architecture to reach mobile or fixed final individual client.

To the best of our knowledge, there is no theoretical research that investigates the performance of the mm-wave backhaul networks. Motivated by the lack of study and by our TWEETHER project, in this paper we carry out the analytical study for the P2MP aided mm-wave backhaul network, and enable an energy and spectrum efficient backhaul architecture for future. The main contributions can be summarized as follows.

- We propose the novel mm-wave backhaul solution by leveraging the P2MP technique in order to boost high capacity of future wireless systems. A tractable stochastic geometry model is proposed for analyzing the performance of the P2MP assisted mm-wave backhaul network conceived in this paper. Two different theoretical models are developed: one is the general P2MP assisted mm-wave backhaul network (GBN) model with the objective of comprehensively evaluating performance, and the other is the simplified P2MP mm-wave backhaul network (SBN) model for analyzing the dominant performance factors including the LOS interference and path loss.
- We carry out novel performance analysis for both the GBN and SBN models, and derive the exact-form expressions for the SINR coverage probability, which can reflect communication reliability of desired link. Furthermore, by using the Gaussian-Chebyshev quadrature and the intelligent manipulations, the closed-form expressions of the SINR coverage probability can be obtained for the GBN and SBN models. The analytical results imply that the LOS interference will be a dominant effect on the coverage rate performance of the backhaul networks.
- With the help of the stochastic geometry assisted tractable model, we investigate the trade-off between energy-efficiency (EE) and area spectral-efficiency (ASE) of our P2MP mm-wave backhaul networks. The original non-convex optimization problem is analyzed and solved by the proposed algorithm, thereby resulting in the optimal power control strategy. With the aid of this strategy, the best trade-off between EE and ASE is obtained for our mm-wave backhaul networks.
- We carry out a range of performance evaluation for the P2MP mm-wave backhaul networks. For the SINR coverage probability of the networks, the exact- and closed-form analytical results under the GBN and SBN models are validated and well agree with those obtained by Monte-Carlo simulations. According to the performance evaluation, our proposed P2MP mm-wave backhaul is shown to be a promising solution for future wireless systems, owing to the significant ASE performance gain benefited from using P2MP technique over traditional P2P, as well as the huge rate improvement by leveraging the mm-wave communications rather than conventional UHF.

II. System Model

A. Network Structure

We consider a point-to-multipoint (P2MP) mm-wave backhaul network, which consists of multiple hubs (as macro base stations) of each serving several small-cell base stations (SCBSs). Fig. 1 shows a simple example of our P2MP mm-wave backhaul network model which has three neighboring hubs. Note that, Fig. 1(a) gives the schematic for an example of the mm-wave backhaul network, and Fig. 1(b) depicts the

[1]TWEETHER stands for traveling wave tube based W-band wireless networks with high data rate, distribution, spectrum and energy efficiency.

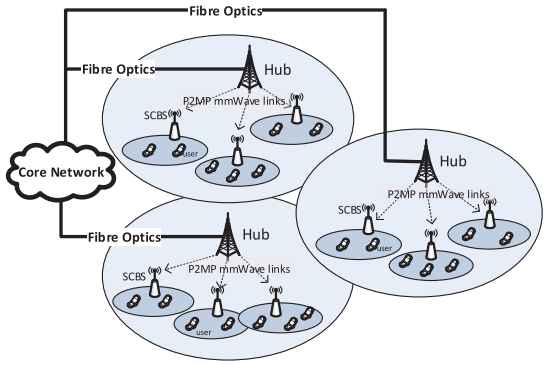

(a) Schematic of network model

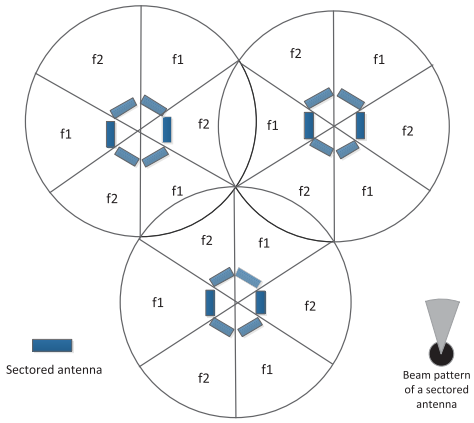

(b) P2MP architecture

Fig. 1. An example of P2MP aided mm-wave backhaul network model.

conceptual structure of P2MP architecture employed by the example network.

In Fig. 1(a), we assume that, all hubs are connected to core network via fibre optic links. Each of the hubs can support a cluster of SCBSs, and neighboring hubs' service areas may geographically overlap with each other. We assume that, the mm-wave backhaul transmissions from each hub to its SCBSs are based on time division multiple access (TDMA) scheme. The P2MP mm-wave links are established for backhaul transmission from each hub to its SCBSs, as shown by Fig. 1(b), where a service area of a hub can be envisioned as a circle with multiple sectors. Each of the hubs, seating at the origin of each circle, employs multiple sectored antennas of each serving the SCBSs in the corresponding sector area. When TDMA is assumed, every sectored antenna of a hub can serve one SCBS within its sector area at a time. In that case, each hub can simultaneously transmit information to multiple SCBSs, each of which is supported by one sectored antenna. Compared to traditional point-to-point (P2P) approach, a P2MP is capable of increasing link utilization, and reducing communication latency as well as achieving higher network throughput [14]. This is because that, our P2MP approach can allow a hub to support multiple links at a time, whereas the P2P can not. Furthermore, a P2MP approach demands lower hardware cost for a single link than a P2P one, thereby achieving a significant saving for the total cost of ownership (TCO).

Without loss of generality, in this paper, each hub is assumed to have 6 sectored antennas. In order to achieve a good trade-off between interference avoidance and spectral efficiency, the frequency reuse pattern in Fig. 1(b) is employed, where the transmissions in every two neighboring sectors are allocated the orthogonal frequency bands f_1 and f_2, each of which has a bandwidth B_0. For theoretical study, the radio characteristic of a sectored antenna can be modeled as the bottom-right plot of Fig. 1(b), where a main lobe beam and a side lobe beam are labeled by light and dark colors, respectively. The beam pattern, $\Psi(M, m, \theta)$, can be characterized by three values: main lobe gain M, side lobe gain m, and main lobe beamwidth θ. The main lobe beamwidth of each sectored antenna is constrained to be $\theta \leq 120^\circ$, so that inter-sector interference is minimized.

With the aid of stochastic geometry approach, a tractable analytical network model is proposed for characterizing the performance of our mm-wave P2MP backhaul networks. Without loss of generality, the backhaul network is modeled as one circle, denoted by $\mathcal{S}$ with radius R, where the typical SCBS seats at the origin $(0, 0)$ and its serving hub locates at $(0, D_0)$. The other hubs in the network are seen as interfering hubs of the typical SCBS. Known from [29] and [30], the locations of interfering hubs distributed on the circle area can be modeled as a homogenous Poisson point process (PPP) Φ of intensity λ. The PPP assumption can be justified by the fact that nearly any hub distribution in a 2-D plane results in a small fixed SINR shift relative to the PPP [11]. Specifically, we would like to clarify that, a homogeneous PPP is employed to approximate a non-homogeneous PPP or a binomial point process (BPP), as long as the network size is sufficiently large (such that $R \geq$ 2km assumed in our simulation) so that the boundary effect can be negligible. As an interesting future research, we will apply the BPP model to the mm-wave backhaul networks with limited size for precisely investigating the boundary effect. According to [31], a 2-D plane for the PPP assumption could be an infinite area or a finite area such as a circle area assumed in this paper. Note that, we analyze the performance for the typical SCBS while our results hold for other SCBSs in the P2MP mm-wave backhaul network according to Slivnyak Theorem[2] [31], [32]. By leveraging Slivnyak theorem, it allows us to randomly select the typical SCBS in the network, without changing its statistical properties. Note that, we assume that our backhaul network has been optimized, where each SCBS is associated with the best hub and is able to support its access links. In this paper we only focus on backhaul transmission.

B. Propagation and Blockage Model

Directional beamforming is assumed for each link, where main lobe beam is aligned towards the dominate propagation path. Assume that, each sectored antenna of all hubs has the

[2]Slivnyak theorem: for a PPP Φ, conditioning on a point at x does not change the distribution of the rest of the process, since the independence among all the points.

same beam pattern of $\Psi(M_t, m_t, \theta_t)$, and each SCBS has the same pattern of $\Psi(M_r, m_r, \theta_r)$. Upon performing perfect beam alignment, the effective antenna gain of the desired communication link for the typical SCBS becomes

$$G_0 = M_t M_r \tag{1}$$

which is for analysis tractable. Owing to operating on the same frequency band, the typical SCBS will suffer from intra-hub interferences (IntraHI) caused by the serving hub and inter-hub interferences (InterHI) caused by the interfering hubs. As shown by Fig. 1(b), the main lobe beams for the desired link and its two IntraHI links are separated by at least of 60°. Therefore, for the desired link, the effective antenna gain imposed by an IntraHI link can be modelled as

$$G_{0,j} = m_t M_r, \quad \forall j \in \{1, 2\}, \tag{2}$$

where subscript 0 denotes the serving hub, and subscript j is index of an IntraHI sectored antenna.

By contrast, for the desired link, the effective antenna gains imposed by the three InterHI links of an interfering hub are discrete random variables according to

$$\begin{aligned}
&(\tilde{G}_{i,j}, \forall j \in \{1,2,3\}) \\
&= (\tilde{G}_{i,1}, \tilde{G}_{i,2}, \tilde{G}_{i,3}) \\
&= \begin{cases}
(M_t M_r, M_r m_t, M_r m_t), & \text{w.p. } p_1 = 3\theta_t\theta_r/4\pi^2 \\
(m_t M_r, m_t M_r, m_t M_r), & \text{w.p. } p_2 = (2\pi - 3\theta_t)\theta_r/4\pi^2 \\
(M_t m_r, m_t m_r, m_t m_r), & \text{w.p. } p_3 = 3\theta_t(2\pi - \theta_r)/4\pi^2 \\
(m_t m_r, m_t m_r, m_t m_r), & \text{w.p. } p_4 = (2\pi - 3\theta_t) \\
 & \qquad (2\pi - \theta_r)/4\pi^2
\end{cases}
\end{aligned} \tag{3}$$

where subscript i ($i \in \Phi$) is index of an interfering hub, and subscript j is index of an InterHI sectored antenna of the hub.

As illustrated by Fig. 1(b), there are three sectored antennas of an interfering hub using the frequency band same as the typical link. As a result, the desired link has three InterHI links caused by each interfering hub, giving the effective antenna gains $\tilde{G}_{i,1}, \tilde{G}_{i,2}, \tilde{G}_{i,3}$ in (3). They could have four different groups of values, which correspond to four different scenarios. Let us use the first scenario as an example to explain how to obtain the effective antenna gain and the corresponding probability. In the first scenario, we have $\tilde{G}_{i,1} = M_t M_r$, meaning that the main lobe beam of the desired link intersects with the main lobe beam of InterHI link 1 initiated by hub i. Observed from the frequency reuse pattern assumed in Fig. 1(b), for each hub, the main lobe beams of every two sectored antennas operating on the same frequency band are separated by at least 60°. In that case, the main lobe beam of the desired link will only intersect with the side lobe beam of InterHI links 2 and 3 of hub i, thereby giving that $\tilde{G}_{i,2} = \tilde{G}_{i,3} = M_r m_t$. Further, the desired link's sectored antenna has a main lobe beamwidth of θ_r, while each sectored antenna of hub i has a beamwidth θ_t of main lobe, in which $\theta_t, \theta_r \in [0, 2\pi]$ follows uniform distribution. Hence, when considering the main lobe beam of the desired link intersect with *any of the three InterHI* links' main lobe beam, we have the probability, given by

$$p_1 = (\frac{\theta_r}{2\pi}) \times (\frac{\theta_t}{2\pi} + \frac{\theta_t}{2\pi} + \frac{\theta_t}{2\pi}) = \frac{3\theta_t\theta_r}{4\pi^2}. \tag{4}$$

It is straightforward that the other three scenarios will have the effective gains in (3), where the relating probabilities can be deduced similar to that in (4).

When comparing (1) with (3), we readily know that InterHI will be the dominant interference for the typical SCBS, which is due to the following two reasons. First, when employing the P2MP architecture in Fig. 1(b), the main lobe beam of the typical link will be affected by the side lobe beams of the two IntraHI links only. By contrast, the typical link could suffer from a strong interference caused by the main lobe beam of a InterHI link, as illustrated by the first case in (3). In general, sophisticated mm-wave antenna design can enable a result of $M_t \gg m_t$, $M_r \gg m_r$. Hence, the InterHI gain will be much higher than the IntraHI gain. Second, in the mm-wave backhaul networks, the typical SCBS experiences two IntraHI links initiated from its serving hub only, while theoretically it could have the InterHI caused by all the interfering hubs in the network. Specifically, as the density of the hubs increases, the number of InterHI will increase while the number of IntraHI will not. Hence, InterHI will be the dominant effect.

The mm-wave links between the typical SCBS and the hubs can be either line of sight (LOS) or non-line of sight (NLOS). Further, we assume that, the LOS probabilities for different links are independent, and potential correlations of blockages are ignored. Let Φ_L and $\Phi_N = \Phi - \Phi_L$ be the point processes of LOS hubs and NLOS hubs, and are obtained by applying independent thinning on the PPP Φ using the LOS probability $p_L(x)$ to determine whether a link of length x is LOS or not [11]. The intensities of Φ_L and Φ_N are respectively determined by $p_L(x)\lambda$ and $(1 - p_L(x))\lambda$. The LOS probability function $p_L(x)$ only depends on the length of the link, the distribution of the blockage process is stationary and isotropic.

The LOS probability function $p_L(x)$ is mainly related to stochastic blockage parameters, which are characterized by some random distributions. In this paper, the blockages in the networks are modeled by employing a Boolean model of rectangles. In this case, the LOS probability function can be expressed as $p_L(x) = e^{-\beta x}$, where β is a parameter characterized by the statistics of densities and average sizes of blockages in the network. Therefore, we readily know that the probability $p_L(x)$ is a monotonically decreasing function of distance x. The path loss exponent for each link is a discrete random variable given by

$$\alpha_i = \begin{cases} \alpha_L, & \text{w.p. } p_L(x) \\ \alpha_N, & \text{w.p. } 1 - p_L(x). \end{cases} \tag{5}$$

Furthermore, we denote the path loss intercept as $\kappa = 20\log_{10}(\frac{2\pi d_{\text{ref}}}{\phi_{\text{ref}}})$ with $d_{\text{ref}} = 1\text{m}$ and ϕ_{ref} as the carrier wavelength [33, eq. (2.41)].

C. SINR for Desired Link

We assume that the small-scale fading pertaining each link follows independent Nakagami-m fading, where the fading

$$\text{SINR} = \frac{P_t G_0 |h_0|^2 \kappa D_0^{-\alpha_0}}{\sum_{j=1}^{2} P_t G_{0,j} |h_0|^2 \kappa D_0^{-\alpha_0} + \sum_{i>0, i\in\Phi} \sum_{j=1}^{3} P_t \tilde{G}_{i,j} |h_i|^2 \kappa D_i^{-\alpha_i} + N_0} \tag{6}$$

parameters m_L and m_N for the LOS and NLOS are constrained to be integer values for mathematical tractability. In the following, we refer h_0 as the channel gain of the desired link, and h_i, $i \in \mathcal{S}$ as the channel gain of InterHI link. For mathematical tractability, we assume that the small-scale fading gains are the same for the links from a hub to its SCBSs which are served at the same time slot. The background noise is characterized by a zero-mean, complex Gaussian random variable with variance N_0. Based on the assumptions thus far, the overall received SINR at the typical SCBS can be expressed as (6), shown at the top of this page. where P_t is the transmit power of each sectored antenna of a hub, and D_i is the distance from hub i to the typical SCBS. G_0, $G_{0,j}$ and $\tilde{G}_{i,j}$ are defined in (1)–(3), respectively. Note that the SINR in (6) is a random variable, due to the randomness of the hub locations D_i, small-scale fading h_i, and the effective antenna gain $\tilde{G}_{i,j}$. Note that in (6), the first term of the denominator denotes the IntraHI of the typical SCBS, while the second term of the denominator is the InterHI.

D. Performance Metrics

For our P2MP mm-wave backhaul network, we consider a range of performance metrics which include coverage probability, area spectral efficiency (ASE), energy efficiency (EE), etc. The coverage probability is also referred to as the success probability, which reflects the reliability of the link between the typical SCBS and its serving hub. The definition of the coverage probability for the typical SCBS can be expressed as [11] and [34]

$$P_c(T) = \Pr\left(\text{SINR} > T\right) \tag{7}$$

where T denotes the SINR threshold. The coverage probability defined in (7) can be further explained as follows: (i) the probability that a randomly chosen SCBS in the network can achieve the target SINR T; (ii) the average fraction of the SCBSs achieving the target SINR T at any given time; (iii) the average fraction of the network area that is in coverage at any given time. Therefore, the typical SCBS is said to be in coverage if it is able to connect at least one hub in the P2MP mm-wave backhaul networks with SINR above threshold T.

Furthermore, the rate coverage probability $P_{rc}(\Gamma)$ is provided to characterize the exact rate distribution in order to analyze the rate performance of the networks. Given the SINR coverage probability $P_c(T)$, the rate coverage probability can be computed as

$$P_{rc}(\Gamma) = \Pr(\text{Rate} > \Gamma) = P_c(2^{\Gamma/B_0} - 1) \tag{8}$$

where $\Gamma = B_0 \log_2(1+T)$ is the target rate requirement conditioned on the SINR threshold T. Note that, the rate coverage probability enables to show the performance gain achieved by our mm-wave backhaul networks over the traditional UHF networks.

Finally, we define another important performance metric, the EE of the P2MP mm-wave backhaul network, as [34]

$$\eta_{EE} = \frac{B_0 \eta_{ASE}}{P_{tot}} = \frac{P_c(T) B_0 \log_2(1+T)}{\frac{1}{\epsilon} P_t + P_{con}} \tag{9}$$

where η_{ASE} describes the network capacity measured in b/s/Hz/m^2, given by

$$\eta_{ASE} = \hat{\lambda} \hat{N} P_c(T) \log_2(1+T). \tag{10}$$

Note that, $\hat{N}$ denotes the number of links supported by, i.e. the number of SCBSs served by each hub at each time slot, $\hat{\lambda}$ denotes the intensity of the hubs in our backhaul network and $P_{tot} = \hat{\lambda}\hat{N}(\frac{1}{\epsilon} P_t + P_{con})$ is the total transmit power consumed by the network conditioned on the density of hubs. It should be noted that, the ASE characterizes the sum rate of the network in a unit area normalized by bandwidth, and reflects the network capacity according to various densification. Further, ϵ is the amplifier efficiency. We assume the same transmit power P_t and constant circuit power consumption P_{con} for each sectored antenna.

III. Performance Analysis for General P2MP mm-wave Backhaul Networks

In this section, we analyze the SINR coverage probability for the P2MP mm-wave backhaul network under the GBN model. In this case, the LOS and NLOS probabilities of communication links are modeled as the exponential functions in [11]. When all links including desired link and interfering links experience the independent Nakagami-m fading, we first derive the exact expressions for the SINR coverage probability. Further, with the aid of sophisticated approximation methods, we also obtain the closed-form expressions for the coverage probability. In the end, when considering the special scenario that all links experience independent Rayleigh fading, the closed-form expressions for SINR coverage probability are derived.

Based on Total Probability Theorem, the SINR coverage probability of typical SCBS is

$$P_c(T) = \sum_{s\in\{L,N\}} \Pr\left(\text{SINR} > T | \alpha_0 = \alpha_s\right) \Pr(\alpha_0 = \alpha_s) \tag{11}$$

where $\Pr(\text{SINR} > T | \alpha_0 = \alpha_s)$ are the conditional probabilities on the event that the desired communication link is either LOS or NLOS, respectively. As discussed in Section II, the probabilities of the desired link being LOS and NLOS can be given by

$$\Pr(\alpha_0 = \alpha_L) = e^{-\beta D_0} \quad \text{and} \quad \Pr(\alpha_0 = \alpha_N) = 1 - e^{-\beta D_0}. \tag{12}$$

Let us denote $I_\Phi = \sum_{i>0, i\in\Phi} \sum_{j=1}^{3} P_t \tilde{G}_{i,j} |h_i|^2 \kappa D_i^{-\alpha_i}$ as the total InterHI observed by the typical SCBS, which can

be easily known from (6). Then, the conditional probabilities $\Pr(\text{SINR} > T|\alpha_0 = \alpha_l), s \in \{L, N\}$ can be written as

$$\Pr(\text{SINR} > T|\alpha_0 = \alpha_s) = \int_0^\infty \Pr\left(|h_0|^2 > A_s(x + N_0)\right) \times f_{I_\Phi}(x)dx, \quad (13)$$

which are obtained by assuming the condition: $P_t G_0 > T\sum_{j=1}^{2} P_t G_{0,j}$, otherwise, the probabilities in (13) become zeros. Above, A_L and A_N can be given by

$$A_L = \frac{TD_0^{\alpha_L}}{\kappa(P_t G_0 - T\sum_{j=1}^{2} P_t G_{0,j})},$$
$$A_N = \frac{TD_0^{\alpha_N}}{\kappa(P_t G_0 - T\sum_{j=1}^{2} P_t G_{0,j})}. \quad (14)$$

In (13), $f_{I_\Phi}(x)$ represents the PDF of the InterHI for the typical SCBS. Here, in order to derive the probabilities in (13), we introduce the following proposition.

Proposition 1 [11]: The CDF of a Nakagami-m distributed random variable X with an integer parameter m can be closely approximated as

$$F_X(x) \approx \left(1 - e^{-ax}\right)^m \quad (15)$$

where $a = m(m!)^{-1/m}$.

Proof: See the proofs in [11, Lemma 6]. ∎

Therefore, with the aid of Proposition 1, we can rewrite the conditional probabilities $\Pr(\text{SINR} > T|\alpha_0 = \alpha_s)$ as

$$\begin{aligned}&\Pr(\text{SINR} > T|\alpha_0 = \alpha_s)\\ &= 1 - \int_0^\infty \Pr\left(|h_0|^2 < A_s(x + N_0)\right) f_{I_\Phi}(x)dx,\\ &\approx 1 - \int_0^\infty \left(1 - e^{-a_s A_s(x+N_0)}\right)^{m_L} f_{I_\Phi}(x)dx. \quad (16)\end{aligned}$$

Upon applying some specific calculations on the equations, an exact expression of the coverage probability can be characterized in the following theorem.

Theorem 1: When assuming independent Nakagami-m fading channels, the exact-form expression of the SINR coverage probability $P_c(T)$ for the P2MP mm-wave backhaul networks under the GBN model can be obtained by (17), shown at the bottom of this page.

Proof: See Appendix A. ∎

However, the exponent terms in (17) generally require numerical evaluation of the integral. As shown in the above equation, there are 32 number of the integral terms to compute for the best case of $M_L = M_N = 1$. As the values of M_L and M_N get bigger, the number of the integral terms in the equation will significantly increases and, hence, it becomes more challenging to analyze. To derive the accurate coverage probability result based on (17), it demands extensive Monte-Carlo simulations. For this sake, we further derive the closed-form expression in the following theorem.

Theorem 2: When assuming independent Nakagami-m fading channels, the closed-form expression of the SINR coverage probability $P_c(T)$ for the P2MP mm-wave backhaul networks under the GBN model can be given by

$$\begin{aligned}&P_c^{(\text{GBN})}(T)\\ &\approx \sum_{r=1}^{m_L}\binom{m_L}{r}(-1)^{r+1}e^{-ra_L A_L N_0 - \beta D_0}\\ &\quad\times\prod_{k=1}^{4} e^{-2\pi\lambda p_k(J_1(k)+J_2(k))}\\ &\quad+\sum_{s=1}^{m_N}\binom{m_N}{s}(-1)^{s+1}e^{-sa_N A_N N_0}(1 - e^{-\beta D_0})\\ &\quad\times\prod_{k=1}^{4} e^{-2\pi\lambda p_k(J_3(k)+J_4(k))} \quad (18)\end{aligned}$$

where A_L and A_N are given by (14). In (18), $J_1(k)$–$J_4(k)$ can be computed as

$$\begin{aligned}J_1(k) &\approx \frac{\pi R}{2U}\sum_{u=1}^{U}\sqrt{1-\theta_u^2}\psi_u e^{-\beta\psi_u}\\ &\quad\times\left(1 - \left(1 + \frac{ra_L A_L\sum_{j=1}^{3} P_t Q_{j,k}\kappa}{\psi_u^{\alpha_L} m_L}\right)^{-m_L}\right), \quad (19)\\ J_2(k) &\approx \frac{\pi R}{2U}\sum_{u=1}^{U}\sqrt{1-\theta_u^2}\psi_u(1 - e^{-\beta\psi_u})\\ &\quad\times\left(1 - \left(1 + \frac{ra_L A_L\sum_{j=1}^{3} P_t Q_{j,k}\kappa}{\psi_u^{\alpha_N} m_N}\right)^{-m_N}\right), \quad (20)\\ J_3(k) &\approx \frac{\pi R}{2U}\sum_{u=1}^{U}\sqrt{1-\theta_u^2}\psi_u e^{-\beta\psi_u}\\ &\quad\times\left(1 - \left(1 + \frac{sa_N A_N\sum_{j=1}^{3} P_t Q_{j,k}\kappa}{\psi_u^{\alpha_L} m_L}\right)^{-m_L}\right), \quad (21)\end{aligned}$$

$$\begin{aligned}&P_c^{(\text{GBN})}(T)\\ &\approx \sum_{r=1}^{m_L}\binom{m_L}{r}(-1)^{r+1}e^{-ra_L A_L N_0 - \beta D_0}\prod_{k=1}^{4} e^{-2\pi\lambda p_k\int_0^R\left(1-1/(1+\frac{ra_L A_L\sum_{j=1}^{3} P_t Q_{j,k}\kappa}{x^{\alpha_L} m_L})^{m_L}\right)e^{-\beta x}xdx}\\ &\quad\times\prod_{k=1}^{4} e^{-2\pi\lambda p_k\int_0^R\left(1-1/(1+\frac{ra_L A_L\sum_{j=1}^{3} P_t Q_{j,k}\kappa}{x^{\alpha_N} m_N})^{m_N}\right)(1-e^{-\beta x})xdx} + \sum_{s=1}^{m_N}\binom{m_N}{s}(-1)^{s+1}e^{-sa_N A_N N_0}(1 - e^{-\beta D_0})\\ &\quad\times\prod_{k=1}^{4} e^{-2\pi\lambda p_k\int_0^R\left(1-1/(1+\frac{sa_N A_N\sum_{j=1}^{3} P_t Q_{j,k}\kappa}{x^{\alpha_L} m_L})^{m_L}\right)e^{-\beta x}xdx}\prod_{k=1}^{4} e^{-2\pi\lambda p_k\int_0^R\left(1-1/(1+\frac{sa_N A_N\sum_{j=1}^{3} P_t Q_{j,k}\kappa}{x^{\alpha_N} m_N})^{m_N}\right)(1-e^{-\beta x})xdx} \quad (17)\end{aligned}$$

$$J_4(k) \approx \frac{\pi R}{2U} \sum_{u=1}^{U} \sqrt{1-\theta_u^2}\psi_u(1-e^{-\beta\psi_u}) \times\left(1-\left(1+\frac{sa_N A_N \sum_{j=1}^{3} P_t Q_{j,k}\kappa}{\psi_u^{\alpha_N} m_N}\right)^{-m_N}\right), \quad (22)$$

where $a_L = m_L(m_L!)^{-1/m_L}$, $a_N = m_N(m_N!)^{-1/m_N}$, $\psi_u = \frac{(\theta_u+1)R}{2}$, and $\theta_u = \cos(\frac{2u-1}{2U}\pi)$ are the Gaussian-Chebyshev nodes over interval $[-1, 1]$. The parameter U is Gaussian-Chebyshev parameters, and it denotes the number of series expansion terms for Gauss-Chebyshev quadrature. In addition, the parameter U relates to the trade-off between accuracy and complexity for (18).

Proof: See Appendix B. ■

To the best of our knowledge, stochastic geometry approach based performance analysis on mm-wave networks, the existing literatures have derived the very complicated integral results for coverage probability, which are unable to derive useful insights for theoretical studies and practical system design. By contrast, in this paper, it is the first novel work that derives the closed-form expressions of the SINR coverage probability for the mm-wave backhaul networks. In comparison to the result in Theorem 1, the SINR coverage probability provided by Theorem 2 significantly reduces the computation complexity for evaluating the network performance. The probability result in Theorem 2 does not have the integral terms, and is easy to compute, due to the simple forms which consist of power functions, fractional functions, and exponential functions.

In addition, according to Theorem 2, we are now able to deduce the following implications. In (18), the the first exponential terms, $e^{-A_L N_0}$ and $e^{-A_N N_0}$, of the two summations reflect the noise effects conditioned on the desired link is LOS and NLOS, respectively. Furthermore, observed from the product terms in (18), $J_1(k)$ and $J_3(k)$ correspond to the effect of the LOS interferences, while $J_2(k)$ and $J_4(k)$ refer to the effect of the NLOS interferences. Note that, the interference effects are evaluated by different antenna gains defined in (3). By comparing $J_1(k)$ (and $J_3(k)$) with $J_2(k)$ (and $J_4(k)$), we readily find that, the LOS interferences have a much bigger effect on the coverage probability than the NLOS interferences. When the LOS interference gets closer the typical SCBS, it could be the dominant factor of the performance degradation. Furthermore, the accuracy of the closed-form expressions in Theorem 2 can be validated by comparing with the exact-form results in Theorem 1. Correspondingly, we derive the following remark.

Remark 1: By employing the Gaussian-Chebyshev approximation, the closed-form expression (18) for the coverage probability generally provides a near-optimal approximation of the probability in (17) when the Gaussian-Chebyshev parameter U is appropriately chosen such as $U \geq 10$. Therefore, the analytical results derived in (18) are more efficient to compute, instead of numerical evaluation of the integral in (17).

Table I provides the numerical comparison of the coverage probabilities characterized by the integral result of Theorem 1 and the closed-form result of Theorem 2, where the main parameters can be found in the beginning of Section VI.

TABLE I

COMPARISON OF ANALYTICAL RESULTS BY THEOREM 1 AND THEOREM 2, WHERE $D_0 = 150$, $M_L = 3$ AND $M_N = 2$

SINR threshold (dB)	$T=-5$	$T=5$	$T=15$	$T=25$
$P_c(T)$ in (17)	0.8038	0.7497	0.6762	0.3782
$P_c(T)$ in (18), $U=5$	0.8244	0.7701	0.6968	0.3867
$P_c(T)$ in (18), $U=8$	0.8055	0.7594	0.6808	0.3798
$P_c(T)$ in (18), $U=10$	0.8046	0.7515	0.6801	0.3799
$P_c(T)$ in (18), $U=15$	0.8042	0.7507	0.6777	0.3791
$P_c(T)$ in (18), $U=20$	0.8039	0.7499	0.6767	0.3793
$P_c(T)$ in (18), $U=25$	0.8039	0.7498	0.6765	0.3787
$P_c(T)$ in (18), $U=30$	0.8039	0.7498	0.6764	0.3787

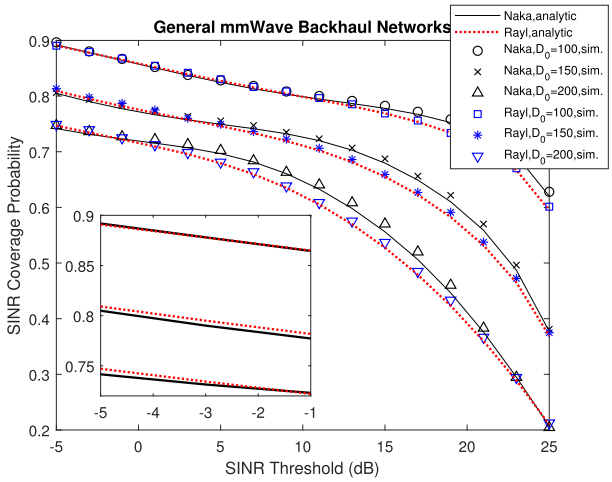

Fig. 2. Coverage probability against SINR threshold T for the mm-wave P2MP backhaul networks, validation of analytical results for the GBN model when all the links experience Nakagami-m fading and Rayleigh fading respectively.

Note that, all the values in Table I are analytical results, which are all based on using the approximated Nakagami-m CDF introduced in Proposition 1. Furthermore, the results of the second row in the table are obtained by Theorem 1 without using Gaussian-Chebyshev approximation, while the results of the other rows are derived by Theorem 2 with employing Gaussian-Chebyshev approximation. In order to show the approximation tightness of Proposition 1, we compare the results derived by Theorem 1 (i.e. the second row of Table I) with the Monte-Carlo simulation results in Fig. 2 which can be used to reflect the coverage probability based on the exact Nakagami-m CDF. In Table I, it is observed that the approximation by Gaussian-Chebyshev quadrature with $U \geq 10$ agrees well with the exact integral expression, thus validating the efficiency and accuracy of the closed-form expression. This can be understood by the fact that the approximation of Gaussian-Chebyshev quadrature is shown to be exact when using more points U [36]. Furthermore, we note that the closed-form result slightly deviates from the exact integral result when U is relatively small, such as $U = 5$. We also observe that the difference between our closed-form result and the integral result becomes slightly more fluctuating when the target SINR increases. Therefore, the Gaussian-Chebyshev quadrature parameters should be properly selected to yield the near-optimal approximation.

Known from (6), the SINR gets larger as the fading condition of interfering links becomes worse, while it does not monotonically decrease as the fading condition of interfering links become worse due to the existence of the first term in the denominator. Hence, it is worth investigating the SINR coverage probability for the special scenario, when all the links including desired link and interfering links experience independent Rayleigh fading. The following corollary gives the SINR coverage probability of the typical SCBS when assuming the special case.

Corollary 1: When assuming independent Rayleigh fading channels, which corresponds to a rich scattering environment, the closed-form expression of the coverage probability $P_c(T)$ for the dipole model can be given by

$$P_c^{(\mathrm{GBN})}(T) = e^{-A_L N_0 - \beta D_0} \prod_{k=1}^{4} e^{-2\pi\lambda p_k(\tilde{J}_1(k)+\tilde{J}_2(k))} + e^{-A_N N_0}(1-e^{-\beta D_0}) \prod_{k=1}^{4} e^{-2\pi\lambda p_k(\tilde{J}_3(k)+\tilde{J}_4(k))}, \quad (23)$$

where $J_1(k)$–$J_4(k)$ can be found as

$$\tilde{J}_1(k) \approx \frac{\pi R}{2U} \sum_{u=1}^{U} \sqrt{1-\theta_u^2}\psi_u e^{-\beta\psi_u} \times A_L\kappa \sum_{j=1}^{3} P_t Q_{j,k}/(\psi_u + A_L\kappa \sum_{j=1}^{3} P_t Q_{j,k}), \quad (24)$$

$$\tilde{J}_2(k) \approx \frac{\pi R}{2U} \sum_{u=1}^{U} \sqrt{1-\theta_u^2}\psi_u (1-e^{-\beta\psi_u}) \times A_L\kappa \sum_{j=1}^{3} P_t Q_{j,k}/(\psi_u + A_L\kappa \sum_{j=1}^{3} P_t Q_{j,k}), \quad (25)$$

$$\tilde{J}_3(k) \approx \frac{\pi R}{2U} \sum_{u=1}^{U} \sqrt{1-\theta_u^2}\psi_u e^{-\beta\psi_u} \times A_N\kappa \sum_{j=1}^{3} P_t Q_{j,k}/(\psi_u + A_N\kappa \sum_{j=1}^{3} P_t Q_{j,k}), \quad (26)$$

$$\tilde{J}_4(k) \approx \frac{\pi R}{2U} \sum_{u=1}^{U} \sqrt{1-\theta_u^2}\psi_u (1-e^{-\beta\psi_u}) \times A_N\kappa \sum_{j=1}^{3} P_t Q_{j,k}/(\psi_u + A_N\kappa \sum_{j=1}^{3} P_t Q_{j,k}). \quad (27)$$

In above, $\psi_u = \frac{(\theta_u+1)R}{2}$ and $\theta_u = \cos(\frac{2u-1}{2U}\pi)$, while A_L, A_N can be found in (14). Note that, U is the parameters denoting the number of series expansion terms for Gauss-Chebyshev quadrature.

Proof: See Appendix C. ∎

In Corollary 1, we readily obtain the observations similar to those in Theorems 1 and 2. Known from (23)–(27), $\tilde{J}_1(k)$ and $\tilde{J}_2(k)$ reflect the LOS interference, while $\tilde{J}_3(k)$ and $\tilde{J}_4(k)$ reflect the NLOS interference. Interestingly, when $D_0 \geq 10$ and $\alpha_N - \alpha_L \geq 2$, we have that $\tilde{J}_1(k) \gg \tilde{J}_3(k)$, $\tilde{J}_2(k) \gg \tilde{J}_4(k)$ regardless of other parameters of interest. Combining this observation and those from Theorem 2, we are able to deduce the following lemma.

Lemma 1: Regardless of desired link being LOS or NLOS, the LOS interference is the dominant effect on the SINR coverage probability for general P2MP mm-wave backhaul networks.

IV. Coverage Probability Analysis for Simplified P2MP mm-wave Backhaul Networks

In this section, we specialize our analysis to the simplified P2MP mm-wave backhaul network (SBN) model, in order to characterize the key factors of performance degradation. Known from Lemma 1, the LOS interference has a much larger affect on the network performance in comparison to the NLOS interference. Further, the studies in [9] and [10] concluded the simple fact that, the influence of path loss and LOS path on the various performance metrics is found to be almost deterministic in practical mm-wave backhaul networks. Motivated by the above findings, our SBN model are proposed to ignore both the impact of the small-scale fading and the NLOS path, so that the performance analysis can be carried out more concisely, while providing more useful insights from both theoretical and practical aspects.

Let us first introduce the system model of the simplified backhaul networks and make the relating assumptions. First of all, we propose to simplify the analysis by approximating a general LOS probability function $p_L(x)$ by a step function. In this regard, we define the function $p_L(x)$ as

$$p_L(x) = \begin{cases} 1, & \text{for } 0 < x < R_b \\ 0, & \text{for } x \geq R_b \end{cases} \quad (28)$$

where R_b is the radius of LOS circle. In general, the LOS probability of a link is taken to be one within the circle area with radius R_b, and the probability becomes zero outside the LOS circle. The above assumption allows us to investigate how the LOS interference affects the performance of our mm-wave backhaul networks. In addition, such a simplification also enables us to efficiently analyze the ASE and EE trade-off in Section V. In the following, we state the above assumption in detail.

Assumption 1: In the context of the SBN model, all the interfering hubs in a circle area with a radius of R_b (which satisfies $R_b \leq R$) have LOS links observed by the typical SCBS. By contrast, the NLOS hubs outside the circle area are ignored. This can be validated by the fact that the path loss of NLOS component will be much more insignificant than that of the LOS component, especially when the exponent α_N for NLOS case is large [37], [38]. Therefore, the performance of the desired link is mainly limited by the LOS interferers.

Remark 2: Based on the above assumption, we readily know that the point process Φ_L for the LOS interfering hubs is obtained by thinning the PPP Φ using the LOS probability given by (28). The average number of the LOS interfering hubs observed by the typical SCBS should be: $\bar{N}_L = \lambda\pi R_b^2$, according to Cambell's formula [31].

Furthermore, in the following, we introduce another important assumption for the mm-wave backhaul networks under the SBN model.

Assumption 2: In the context of the SBN model, all communication links are free of small-scale fading, since the signal power from a mm-wave LOS transmitter is found to be almost deterministic in measurements [9].

Based on the above assumptions, the received SINR of the typical SCBS under the simplified P2MP mm-wave backhaul networks can be expressed as (29), shown at the bottom of this page.

We should note that, the analysis below is based on the fact that assuming $D_0 < R_b$, which means that the desired link is guaranteed to be LOS link.

Let us now analyze the SINR coverage probability of the typical SCBS for the P2MP mm-wave backhaul networks under the SBN case. Considering the specific assumptions 1 and 2, we can derive the following theorem characterizing the SINR coverage probability.

Theorem 3: Given that all links experiencing no fading, the closed-form expression of the SINR coverage probability $P_c(T)$ for the simplified P2MP mm-wave backhaul networks can be obtained by

$$P_c^{(\mathrm{SBN})}(T) \approx \sum_{v=1}^{V} \binom{V}{v} (-1)^{v+1} e^{-v\eta A_L N_0} \prod_{k=1}^{4} e^{-2\pi\lambda p_k \hat{J}(k)}, \tag{30}$$

where $\eta = V(V!)^{-1/V}$. In (30), $\hat{J}(k)$ can be found by

$$\hat{J}(k) = \frac{\pi R_b}{2W} \sum_{w=1}^{W} \sqrt{1-\theta_w^2}\psi_w \left(1 - e^{-\frac{v\eta A_L \sum_{j=1}^{3} P_t Q_{j,k}\kappa}{\psi_w^{\alpha_L}}}\right), \tag{31}$$

where $\theta_w = \cos(\frac{2w-1}{2W}\pi)$, and $\psi_w = \frac{(\theta_w+1)R_b}{2}$. The parameters V and W are Gaussian-Chebyshev parameters, and they denote the number of series expansion terms for Gauss-Chebyshev quadrature.

Proof: See Appendix D. ∎

Remark 3: It is important to point out that the closed-form expression derived by Theorem 3 generally provides an exact lower bound of the coverage probability for the simplified backhaul networks under the dipole scenario. The expression in (30) gives a near-optimum approximation for the coverage probability when more and more terms are employed, i.e. when $V \geq 5$.

In Table II, it provides the numeric comparison of the theoretical analysis derived by Theorem 3 and the corresponding monte-carlo simulation results (obtained by 10^5 realizations). Observed from the table, the analytical results always get closer to the simulation ones as the value of V increases. Furthermore, when the SINR threshold becomes lower, the analytical results have better approximation. For various cases considered, the differences between the analysis and simulation are always ignorable, especially when V is big, such as $V \geq 5$. Hence, the above observations from Table II validate Remark 3.

TABLE II

ACCURACY VALIDATED BY USING DIFFERENT VALUES OF V, WHERE $D_0 = 150$ AND $R_b = 450$

SINR threshold (dB)	$T=-5$	$T=5$	$T=15$	$T=25$
$P_c(T)$ by simulations	0.9948	0.9423	0.7010	0.4802
$P_c(T)$ in (30), $V=1$	0.9739	0.8707	0.6583	0.3674
$P_c(T)$ in (30), $V=3$	0.9916	0.9197	0.6835	0.4320
$P_c(T)$ in (30), $V=5$	0.9934	0.9323	0.6896	0.4559
$P_c(T)$ in (30), $V=8$	0.9944	0.9410	0.6968	0.4753
$P_c(T)$ in (30), $V=10$	0.9947	0.9419	0.6998	0.4783

V. EE AND ASE TRADE-OFF

Based on the analysis in Section III, we study the trade-off between the EE and ASE achieved by our P2MP mm-wave backhaul networks. For the sake of analytical tractable, we assume all the hubs have the same transmit power P_t for each sector antenna. In this section, for theoretical study we aim to find the best strategy to control transmit power, so that the EE and ASE trade-off can be maximized.

Known from the analysis in Section III, increasing the transmit power P_t will increase the SINR coverage probability of the P2MP mm-wave backhaul networks, while increasing the total power consumption. Hence, to maximize the ASE, it is optimal to use the maximum transmit power available for each sector antenna of each hub. By contrast, the EE performance is not monotonically increasing with the transmit power P_t. Therefore, we motivate to maximize the EE and ASE trade-off for the P2MP mm-wave backhaul networks. In the following, we formulate the optimization problem $\mathcal{P}_0$ as

$$\mathcal{P}_0: \quad \max_{P_t} \ \eta_{EE} \tag{32}$$

$$\text{subject to } \eta_{ASE} \geq \eta_{ASE}^{(min)} \tag{33}$$

$$\hat{\lambda}\hat{N}(\frac{1}{\epsilon}P_t + P_{con}) \leq P_{tot}^{(max)} \tag{34}$$

where η_{ASE} and η_{EE} is obtained by substituting the SINR coverage probabilities in Section III into (10) and (9). In problem $\mathcal{P}_0$, we define the final solution denoted by P_t^*. Constraint (33) assumes that the ASE of the network has to satisfy the minimum required ASE which is $\eta_{ASE}^{(min)}$. In (34), it constrains the maximum available power for the network to be $P_{tot}^{(max)}$.

Problem $\mathcal{P}_0$ is a nonlinear fractional programming problem, which is very difficult to solve. In order to find promising solution to problem $\mathcal{P}_0$, we propose to apply the dinkelbach method [39] to this problem. With the aid of introducing a new variable q, we can convert the original objective function to

$$F(q) = B_0\eta_{ASE}(P_t) - q\hat{\lambda}\hat{N}(\frac{1}{\epsilon}P_t + P_{con}), \quad P_t \in \mathcal{A}, \tag{35}$$

where $\mathcal{A} = \{P_t \mid \eta_{ASE} \geq \eta_{ASE}^{(min)}, \hat{\lambda}\hat{N}(\frac{1}{\epsilon}P_t + P_{con}) \leq P_{tot}^{(max)}\}$. Known from [39], the optimal solution P_t^*

$$\mathrm{SINR} = \frac{P_t G_0 \kappa D_0^{-\alpha_L}}{\sum_{j=1}^{2} P_t G_{0,j}\kappa D_0^{-\alpha_L} + \sum_{i>0, i\in\Phi_L}\sum_{j=1}^{3} P_t \tilde{G}_{i,j}\kappa D_i^{-\alpha_L} + N_0}. \tag{29}$$

can be found by finding the optimal q^* that satisfies $F(q^*) = 0$. When updating variable q iteratively, such as $q_{n+1} = B_0\eta_{ASE}(P^*_{t,n})/\hat{\lambda}\hat{N}(\frac{1}{\epsilon}P^*_{t,n} + P_{con})$ for the $(n+1)$th iteration, $F(q^*)$ will converge to 0 and the final solution of P_t can be obtained, which is proved in [39]. To solve problem $\mathcal{P}_0$, we can iteratively solve the converted optimization problem of $\mathcal{P}_0$, given the variables $P_{t,n}$ and q_n for the nth iteration.

$$\mathcal{P}_1:$$

$$\max_{P_{t,n}} \; F(q_n, P_{t,n}) = B_0\eta_{ASE}(P_{t,n}) - q_n\hat{\lambda}\hat{N}(\frac{1}{\epsilon}P_{t,n} + P_{con})$$
$$\text{subject to (33) and (34).} \tag{36}$$

After converting to the optimization problem of $\mathcal{P}_1$, we can have the following *lemma*.

Lemma 2: For our P2MP mm-wave backhaul networks under the SBN, each sub-problem during an iteration under the converted problem of $\mathcal{P}_1$ is a concave problem, and the value of objective function $F(q_n, P_{t,n})$ converges to 0.

Proof: See Appendix E. ∎

For the P2MP mm-wave backhaul networks, we propose the novel power control algorithm, given by Algorithm 1, which aims to maximize the trade-off between the EE and ASE.

Algorithm 1 Proposed Power Control Algorithm

1: Initialization: (1) Set index $n = 1$, (2) Set maximum iteration number n_{max}, (3) Set $\epsilon > 0$, (4) Set $q_n = 0$;
2: **while** $n <= n_{max}$
3: (A): Solve optimization problem $\mathcal{P}_1(q_n)$ by interior point method;
4: (B): Derive the solution of ith iteration: $P^*_{t,n}$;
5: (C): Compute the value of the objective function $F(q_n, P^*_{t,n})$;
6: **if** $F(q_n, P^*_{t,n}) > \epsilon$ **then**
7: Update $q_n \leftarrow B_0\eta_{ASE}(P^*_{t,n})/\lambda(\frac{1}{\epsilon}P^*_{t,n} + P_{con})$;
8: Set $n \leftarrow n + 1$;
9: Go back to (A);
10: **else**
11: **Output:** the optimal variable $P^*_t = P^*_{t,n}$;
12: **end**
13: **end**

VI. Numerical Simulation

In this section, we first show and discuss the numerical results for the SINR coverage probability of both the GBN and SBN models. Then we evaluate the ASE performance of the backhaul networks. Finally, we present the EE and ASE trade-off for our backhaul networks. Note that, we assume that the mm-wave backhaul networks operate at W band, and each of the two frequency bands f_1 and f_2 has the available bandwidth of B_0. For theoretical study, we assume that the noise power of each link is assumed to be the same, which is σ^2 (dBm/Hz). Further, each link in the network have the independent probability of being LOS and NLOS, and experience independent fading. In the following figures, the main simulation parameters are summarized in Table III if they are not specified.

TABLE III
Simulation Parameters for mm-Wave Backhaul Network

Parameter	Value	Parameter	Value
f_c	94 GHz	B_0	500 MHz
R	2 km	σ^2	-124 dBm/Hz
m_L	3	m_N	2
α_L	2	α_N	4
M_t	15 dB	m_t	-15 dB
M_r	3 dB	m_r	-3 dB
λ	4×10^{-6} hubs/m^2	β	0.008

A. SINR Coverage Probability Performance

In this section, we provide the numerical results to validate the SINR coverage probability derived for the GBN and SBN models in Sections III and IV, respectively. Further, when considering the various simulation scenarios, we comprehensively evaluate the SINR coverage probability of our mm-wave networks, and discuss the implications on practical network design. Note that, we assume that, for the GBN model, the communication links experience either independent Nakagami-m fading or independent Rayleigh fading. To guarantee high-accuracy, all the Monte-Carlo simulation results are obtained from at least 10^5 times of realizations.

Fig. 2 compares the analytical SINR coverage probability results with those obtained by Monte-Carlo simulations for the backhaul networks under the GBN. Seen from the figure, our analytical results perfectly match the simulations under the various scenarios considered, which proves that the analytical SINR distribution for the GBN model is very accurate. In Fig. 2, when the desired link length, i.e. that between the typical SCBS and the serving hub, becomes bigger, the SINR coverage probability decreases, and dramatically drops down in high SINR threshold region. This observation shows the quality of the mm-wave backhaul links high depends on the link length. For supporting relatively long distance transmission, it demands high-quality practical implementation, including optimization of hub location, proper antenna array setup, optimization of available radio resources. Further, the figure also shows that, for medium and high SINR thresholds, the coverage probability is lower bounded by the specific scenario that all links experience independent Rayleigh fading. By contrast, observed from the enlarged subplot of Fig. 2, when the SINR threshold is low and distance D_0 increases, the coverage probability for Rayleigh fading becomes slightly higher than that for Nakagami-m fading. Furthermore, the tightness of Proportion 1 can be evaluated by observing the results in Table I and Fig. 2. Seen from the second row of Table I, we readily know the coverage probability $P_c(T)$ in Theorem 1, which employs Proportion 1 while without using the Gaussian-Chebyshev approximation. When comparing the results of Table I with the corresponding ones of Fig. 2, it finds that there are only up to 0.13% deviation for $-5 \leq T \leq$ 10dB region and up to 0.20% deviation for $10 < T \leq$ 25dB region, respectively. Hence, this observation shows that the approximation introduced by Proportion 1 is relatively tight. From the above observations, we imply that

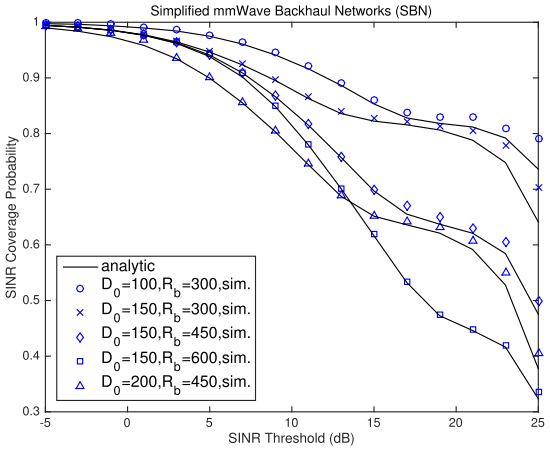

Fig. 3. Coverage probability against SINR threshold T for mm-wave P2MP backhaul networks, validation of analytical results for the SBN model with various R_b values, illustration for the effect of LOS interference on the link reliability.

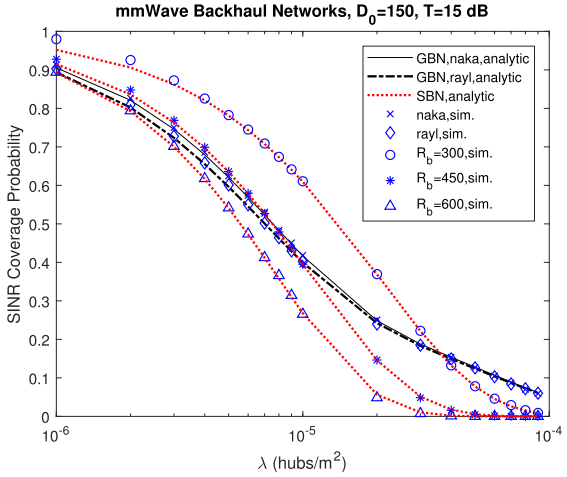

Fig. 4. Coverage probability against intensity λ for mm-wave backhaul networks, validation of analytical results, performance comparison between the GBN model and SBN model, the networks trend to be interference limited as hub density increases.

the link reliability of the mm-wave backhaul network will have more significant effect by fast fading as the link of the communication distance increases.

Next, we validate the analytical results of the SINR coverage probability for the network under the SBN model in Fig. 3. According to the comparison, we prove that, the analytical results perfectly match the simulations under most cases. Nevertheless, there is only a small deviation (less than 6%) between the analytical results and the simulations, when the radius R_b is small. This is because our analysis slightly over-estimates interference effect on the reliability of the backhaul links under the simplified network model. It is worth noting the following important observations when comparing Fig. 3 with Fig. 2. First, the networks under the SBN always achieve a higher SINR coverage probability than the networks under the GBN when the target SINR is small. This implies that, the fast fading and NLOS interference will have a big impact on the network performance when link reliability requirement is high. Second, we observe that, as the length of the desired link increases, the performance gap between the SBN and GBN at the low SINR threshold region becomes bigger. This observation indicates that, the effect of NLOS interference can not be ignored especially when the length of communication link is long. Third, the results for the SBN can match with those for the GBN model in high SINR threshold region when the radius R_b is properly selected, such as $R_b = 450$ for $D_0 = 150$. Also, the SINR coverage probability significantly reduces as radius R_b increases. From the above observations, we may conclude the reliability of backhaul link is heavily affected by neighbouring LOS interfering links especially when high target SINR is required.

In Fig. 4, we evaluate the SINR coverage probability against intensity value λ for the P2MP mm-wave backhaul networks. Once again, the figure shows the analytical results of the SINR coverage probability match with the simulations regardless of network density. Observed from the figure, the reliability of mm-wave backhaul links can be highly affected by interference, and the network exhibits strong interference, when the

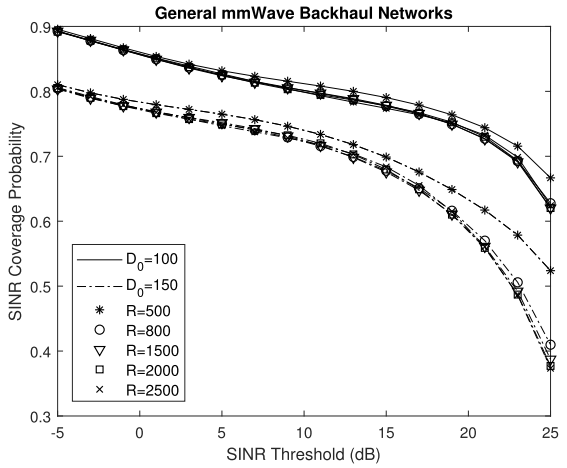

Fig. 5. Coverage probability against SINR threshold T for mm-wave P2MP backhaul networks, evaluation of network size R, the interference outside 0.8km can be ignored.

density of hubs increases. In Fig. 4, under the GBN model, the performance of Rayleigh fading is approaching that of the Nakagami-m when the network density increases. This implies our backhaul networks with relatively high density can be evaluated by ignoring small-scale fading effect. By comparing the results of the GBN with those of the SBN, it derives the observations and conclusions same as those made from Fig. 3. Furthermore, Fig. 5 is shown in order to investigate how the network performance is affected by the network size. Observed from the figure, the coverage probability for the case $D_0 = 100$ will be decreased by less than 1% when the radius R is bigger than 0.8km, while that for the case $D_0 = 150$ will deviate up to 3% only at high SINR threshold region when $R \geq 0.8$km. Moreover, it is also seen that, the curves will become almost the same for the cases of $R \geq 2$km. The above observations imply that, the interference outside 0.8km is very weak, and the network size of $R \geq 2$km is sufficiently large for theoretical study, so that the boundary effect can be ignored.

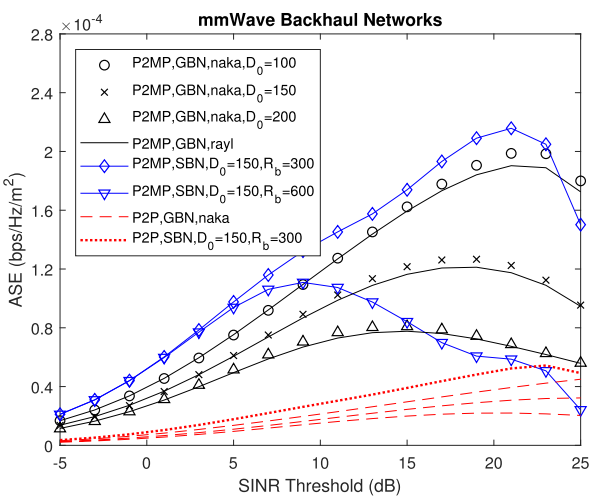

(a) ASE vs T

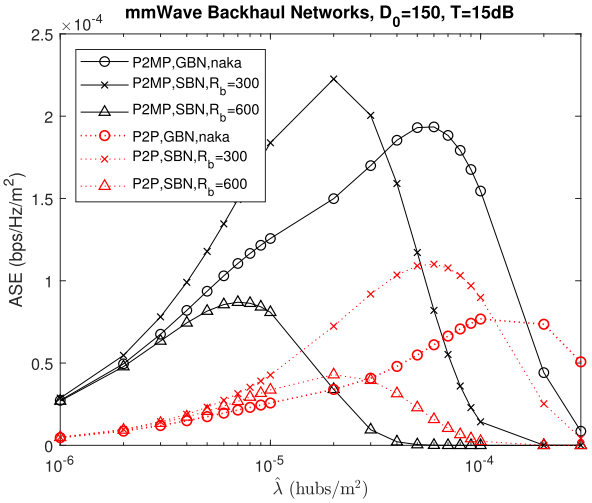

(b) ASE vs λ

Fig. 6. Trade-off between ASE and SINR threshold T as well as that between ASE and intensity λ for mm-wave backhaul networks, ASE performance advantage of novel P2MP over traditional P2P when assuming the same total power consumption.

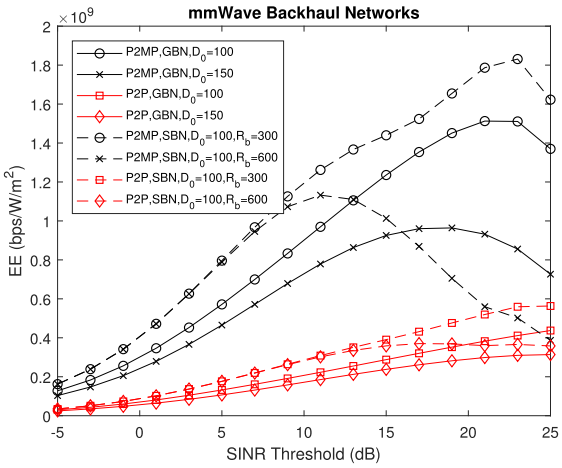

Fig. 7. Trade-off between EE and SINR threshold T for mm-wave backhaul networks, EE performance advantage of novel P2MP technique over traditional P2P one when assuming the same total power consumption, illustration for the effect of LOS interference on EE performance.

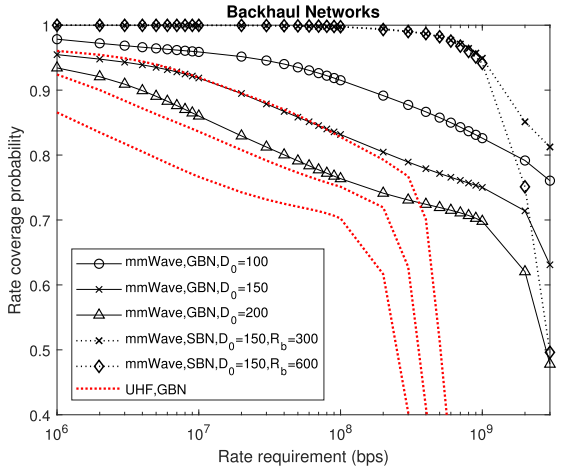

Fig. 8. Rate coverage probability against minimum rate requirement for backhaul networks, rate performance gain achieved by mm-wave aided networks over UHF based networks, rate performance comparison between the GBN model and SBN model.

According to the observations in this section, we conclude that, in contrast to mm-wave access networks, the reliability of our backhaul mm-wave links is more likely dominated by interference (including both LOS and NLOS interference) rather than thermal noise especially when the link length becomes larger. Owing to this, we urge caution that for the argument that mm-wave networks are all noise limited.

B. ASE, EE and Rate Performance

In this section, we investigate and evaluate the ASE and rate performance of the P2MP mm-wave backhaul networks under both the GBN and SBN models. A range of numerical results are provided to validate the advantages of the P2MP architecture employed by our networks over the traditional P2P approach used by the existing networks. To make a fair comparison, we assume the total transmit power and the other power consumption at each hub is the same for both the P2MP and P2P cases. Furthermore, we investigate the performance gain achieved by our proposed networks with mm-wave capability over the ones with traditional UHF links only.

Fig. 6 compares the ASE performance of the P2MP approach aided mm-wave backhaul networks with that of the P2P approach aided networks, when varying the values of SINR threshold and intensity λ, respectively. Note that, in the figure we assume all links experience independent Nakagami-m fading in the context of GBN model. In Fig. 6(a), it clearly observes that the novel P2MP approach can achieve a significantly higher ASE, i.e. average network capacity, than P2P approach for all different SINR thresholds, despite the P2P approach is free of InterHI. This performance gain, that is up to 800%, is due to the fact that multiple SCBSs are served

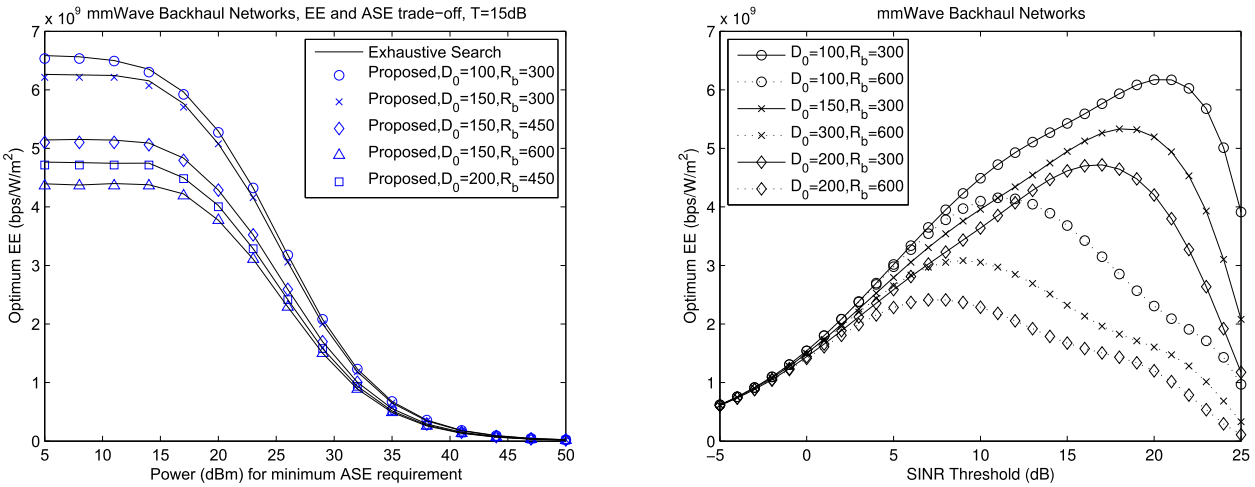

(a) Optimum EE vs $\eta_{ASE}^{(min)}$

(b) Optimum EE vs T

Fig. 9. Optimum EE performance against minimum ASE requirement for mm-wave backhaul networks, performance trade-off between between optimum EE and SINR threshold T, validation of proposed power control algorithm.

by a hub during each time slot. From Fig. 6(a), it also observes that, for the P2MP mm-wave backhaul networks, the optimum ASE is achieved at lower SINR threshold when hubs are located more closer to their SCBSs. Furthermore, for the SBN model, the optimum ASE becomes smaller, and it is obtained at lower SINR threshold as R_b decreases. In contrast, Fig. 6(b) shows the effect of intensity λ on the ASE performance of the backhaul networks, and demonstrates the trade-off between ASE and link reliability (reflected by SINR coverage probability). It is clearly shown that the P2MP approach can significantly outperform the P2P approach, in terms of the optimum ASE. According to comparison, the optimum ASE for the SBN always exists at less dense scenario than that for the GBN. This implies that network capacity are highly affected by strong interference from neighbouring LOS links. Therefore, from Fig. 6, we may conclude that, to design practical mm-wave backhaul networks, it is very important to find the best trade-off between network capacity required and link reliability target, which demands efficiently mitigating interference, carefully managing resource, and optimal hubs deployment.

Fig. 7 investigates the EE performance of the mm-wave backhaul networks with the aid of the P2MP approach as well as the networks with the traditional P2P approach. Note that, for ensuring a fair comparison, we assume that the total power consumed by each hub is the same for both the P2MP and P2P approaches. Regardless of the GBN and SBN models, we clearly observe that the P2MP approach derives significantly better EE performance than the P2P, especially when the length of the typical link D_0 is small. Further, we can see that, there is also a trade-off between the achievable EE and the link reliability. Obviously, to achieve the best trade-off, the novel P2MP approach requires much smaller link reliability than the P2P approach, which enables a lower complexity of receiver design for decoding. The other observations in Fig. 7 are similar to those in Fig. 6, and similar conclusions can be derived. Therefore, we may conclude that, our P2MP aided mm-wave backhaul networks not only achieve significantly higher ASE, but also obtain much better EE, compared to the networks with the P2P approach.

Next, we compare the rate coverage probability of our mm-wave backhaul networks with that of UHF networks in Fig. 8. Note that we assume the UHF network is operated at 2.4 GHz with $B_0 = 50$ MHz available. For the sake of theoretical study, we further assume that the UHF networks can achieve the same antenna gains as those of the mm-wave networks at both hubs and SCBSs. To capture the effect of LOS and NLOS transmissions, we use $\alpha_L = 2$ and $\alpha_N = 3.75$ for the UHF networks. Observed from Fig. 8, the rate performance of backhaul networks with mm-wave capability is significantly improved in comparison with the traditional UHF networks, which is benefited from large bandwidth provided by mm-wave communication. Also, we can clearly see the mm-wave networks are able to support over several Gbps data links when assuming unit transmit power. Furthermore, as known, the achievable antenna gain is related to $G = 4\pi A_e/\lambda_f^2$, where A_e is the aperture of antenna. Hence, the achievable antenna gain will be increased by 20 dB when increasing carrier frequency λ_f^2 ten-fold [13]. In case of operating at low gain, the antenna size for P2MP can be further reduced, with very low footprint. To maintain the same size of antenna aperture, mm-wave backhaul networks will obtain more orders of magnitude rate improvement over UHF backhaul networks. Further, by comparing the results of GBN model with those of the SBN, we observe that mm-wave backhaul communications exhibit interference limited performance if the neighbouring LOS interfering links are not properly managed.

C. Energy Efficiency and ASE Trade-Off

In this section, we investigate the trade-off between EE and ASE for the mm-wave backhaul networks. Due to the

lack of space, we focus on the performance evaluation for the SBN model. The similar observations can be obtained for the GBN model.

Fig. 9 invesigates the performance trade-off between EE and ASE, as well as shows the trade-off between EE and link reliability. In the figure, the optimum EE is derived by solving the optimization problem in $\mathcal{P}_0$. In Fig. 9 (a), it evaluates the optimum EE performance subject to various minimum ASE, which, known by (52), is monotonically increasing with transmit power P_t. From the figure, we can clearly observe the results obtained by the proposed approach agree with those obtained by the exhaustive search, which validates high-efficiency of our method given in Algorithm 1. Further, there always exits a trade-off between the optimum EE and ASE requirement for each case, and the best trade-off can enable higher ASE requirement when D_0 decreases or when the radius of LOS circle R_b becomes smaller. This observation implies that, the mm-wave backhaul networks become less energy efficient demanding more transmit power consumption when the required network capacity gets higher. In Fig. 9 (b), we study the effect of SINR threshold on the EE performance when fixing the minimum ASE $\eta_{ASE}^{(min)} = 0.4 \times 10^{-4}$ bps/Hz/m^2. Observed from Fig. 9 (b), for each scenario there is also a trade-off between EE and link reliability (i.e. SINR coverage probability). Moreover, it is seen that the peak EE increases as the length of the desired link D_0 gets smaller and as the radius of LOS circle R_b decreases. Whereas, in order to achieve the peak EE, it demands higher link reliability when R_b becomes smaller. This observation reflects the fact that, the EE performance of the mm-wave backhaul networks can be significantly degraded by low link reliability and strong neighbouring LOS interfering links. From the above observations, we can conclude that, to achieve the best EE and ASE trade-off, the mm-wave backhaul networks should be designed to limit the communication links, and avoid LOS interferences, while optimizing transmission power.

VII. Conclusion

We have proposed and developed the novel P2MP mm-wave backhaul networks, which are modeled by the tractable stochastic geometry approach for performance analysis. To comprehensively evaluate the network performance, we have proposed two different models including the GBN and SBN. For both the models, a range of exact- and closed-form expressions for the SINR coverage probability have been derived. With the help of the stochastic geometry based tractable model, we have developed the optimal power control algorithm for maximizing the trade-off between EE and ASE performance of our backhaul networks. The analytical results of the SINR coverage probability have been validated by Monte-Carlo simulations. Both the analytical and simulation results have shown that the LOS interference should be avoided or mitigated for our backhaul network to achieve a good coverage probability. The simulation results have shown that, to achieve the best EE and ASE trade-off, the mm-wave backhaul networks should be designed to limit the link distances and LOS interferences, while optimizing the transmission power. Furthermore, according to the performance evaluation, we conclude that our proposed P2MP mm-wave backhaul is a promising solution for future wireless systems.

Appendix A
Proof to Theorem 1

In order to derive the exact expression of the coverage probability, we first give the details of derivations for $\Pr(\text{SINR} > T|\alpha_0 = \alpha_L)$. As known, the binomial theorem is given by $(x-y)^K = \sum_{i=0}^{K} \binom{K}{i}(-1)^{(K-i)}x^i y^{K-i}$.

Upon applying the binomial theorem to (16), $\Pr(\text{SINR} > T|\alpha_0 = \alpha_L)$ can be rewritten as

$$\begin{aligned}
&\Pr(\text{SINR} > T|\alpha_0 = \alpha_L) \\
&\quad = \sum_{r=1}^{m_L} \binom{m_L}{r}(-1)^{r+1} E_{I_\Phi}\left[e^{-ra_L A_L (I_\Phi + N_0)}\right] \\
&\quad \overset{(a)}{=} \sum_{r=1}^{m_L} \binom{m_L}{r}(-1)^{r+1} e^{-ra_L A_L N_0} E_{I_{\Phi_L}}\left[e^{-ra_L A_L I_{\Phi_L}}\right] \\
&\qquad \times E_{I_{\Phi_N}}\left[e^{-ra_L A_L I_{\Phi_N}}\right] \qquad (37)
\end{aligned}$$

where step (a) is due to the fact that the effect of potential blockages is to thin the original PPP I_Φ for interfere hubs into two independent PPPs I_{Φ_L} and I_{Φ_N}, respectively. Note that, $E_{I_{\Phi_L}}\left[e^{-ra_L A_L I_{\Phi_L}}\right]$ for the LOS interference is Laplace functional of I_{Φ_L} [31], given in (38), shown at the bottom of this page.

$$\begin{aligned}
E_{I_{\Phi_L}}\left[e^{-ra_L A_L I_{\Phi_L}}\right] &= E_{|h_{i,j}|^2}\left[E_{D_i}\left[E_{\tilde{G}_{i,j}}\left[e^{-ra_L A_L I_{\Phi_L}}\right]\right]\right] \\
&\overset{(b)}{=} E_{D_i}\left[\sum_{k=1}^{4} p_k E_{|h_{i,j}|^2}\left[e^{-\frac{ra_L A_L \sum_{i>0, i\in\Phi_L}\sum_{j=1}^{3} P_t Q_{i,j,k}\kappa |h_{i,j}|^2}{D_i^{\alpha_L}}}\right]\right] \\
&\overset{(c)}{=} e^{-\lambda \sum_{k=1}^{4} p_k \int_0^{2\pi}\int_0^R \left(1 - E_{|h|^2}\left[e^{-\frac{ra_L A_L \sum_{j=1}^{3} P_t Q_{j,k}\kappa |h|^2}{x^{\alpha_L}}}\right]\right) p_L(x) x dx d\theta} \\
&\overset{(d)}{=} \prod_{k=1}^{4} e^{-2\pi\lambda p_k \int_0^R \left(1 - E_{|h|^2}\left[e^{-\frac{ra_L A_L \sum_{j=1}^{3} P_t Q_{j,k}\kappa |h|^2}{x^{\alpha_L}}}\right]\right) e^{-\beta x} x dx} \\
&\overset{(e)}{=} \prod_{k=1}^{4} e^{-2\pi\lambda p_k \int_0^R \left(1 - 1/(1 + \frac{ra_L A_L \sum_{j=1}^{3} P_t Q_{j,k}\kappa}{x^{\alpha_L} m_L})^{m_L}\right) e^{-\beta x} x dx}. \qquad (38)
\end{aligned}$$

In (38), step (b) follows the total probability theorem, where $\tilde{G}_{i,j} = Q_{i,j,k}$ given by (3). Further, step (c) is obtained by computing the Laplace transform function of the PPP Φ_L. We should note that, in steps (c)-(e), we have $Q_{j,k} = Q_{i,j,k}$ by dropping subscript i for the sake of notational convenience. Moreover, step (d) is derived with the aid of using the polar coordinates in our stochastic geometry based network model. At last, step (e) can be obtained by using the probability generating functional [31].

Similar to the derivations in (38), we can obtain the expression of $E_{I_{\Phi_N}}\left[e^{-ra_N A_N I_{\Phi_N}}\right]$ for NLOS interfering links. Upon substituting the expression of (38) for LOS case and the one for NLOS case into (37), we can obtain

$$\begin{aligned}\Pr(\text{SINR} > T|\alpha_0 = \alpha_L) &= \sum_{r=1}^{m_L} \binom{m_L}{r} (-1)^{r+1} \\ &\times \prod_{k=1}^{4} e^{-2\pi\lambda p_k \int_0^R \left(1-1/(1+\frac{ra_L A_L \sum_{j=1}^{3} P_t Q_{j,k}\kappa}{x^{\alpha_L} m_L})^{m_L}\right) e^{-\beta x} x dx} \\ &\times e^{-ra_L A_L N_0} \\ &\times \prod_{k=1}^{4} e^{-2\pi\lambda p_k \int_0^R \left(1-1/(1+\frac{ra_L A_L \sum_{j=1}^{3} P_t Q_{j,k}\kappa}{x^{\alpha_N} m_N})^{m_N}\right)(1-e^{-\beta x}) x dx}.\end{aligned} \tag{39}$$

Applying the procedures similar to (37)-(39), we are able to derive the expression for the conditional probability $\Pr(\text{SINR} > T|\alpha_0 = \alpha_N)$ as

$$\begin{aligned}\Pr(\text{SINR} > T|\alpha_0 = \alpha_N) &= \sum_{s=1}^{m_N} \binom{m_N}{r} (-1)^{s+1} \\ &\times \prod_{k=1}^{4} e^{-2\pi\lambda p_k \int_0^R \left(1-1/(1+\frac{sa_N A_N \sum_{j=1}^{3} P_t Q_{j,k}\kappa}{x^{\alpha_L} m_L})^{m_L}\right) e^{-\beta x} x dx} \\ &\times e^{-sa_N A_N N_0} \\ &\times \prod_{k=1}^{4} e^{-2\pi\lambda p_k \int_0^R \left(1-1/(1+\frac{sa_N A_N \sum_{j=1}^{3} P_t Q_{j,k}\kappa}{x^{\alpha_N} m_N})^{m_N}\right)(1-e^{-\beta x}) x dx}.\end{aligned} \tag{40}$$

Therefore, Theorem 1 is proved when substituting (39), (40) and (12) into (11).

Appendix B
Proof to Theorem 2

Let us first discuss the derivation procedures for the conditional probability $\Pr(\text{SINR} > T|\alpha_0 = \alpha_L)$, which can be rewritten as

$$\begin{aligned}&\Pr(\text{SINR} > T|\alpha_0 = \alpha_L) \\ &= \sum_{r=1}^{m_L} \binom{m_L}{r} (-1)^{r+1} e^{-ra_L A_L N_0} \\ &\quad \times \prod_{k=1}^{4} e^{-2\pi\lambda p_k J_1(k)} \prod_{k=1}^{4} e^{-2\pi\lambda p_k J_2(k)}.\end{aligned} \tag{41}$$

In (41), $J_1(k)$ and $J_2(k)$ are given by

$$\begin{aligned}J_1(k) = \int_0^R &\left(1 - 1/(1 + \frac{ra_L A_L \sum_{j=1}^{3} P_t Q_{j,k}\kappa}{x^{\alpha_L} m_L})^{m_L}\right) \\ &\times e^{-\beta x} x dx,\end{aligned} \tag{42}$$

$$\begin{aligned}J_2(k) = \int_0^R &\left(1 - 1/(1 + \frac{ra_L A_L \sum_{j=1}^{3} P_t Q_{j,k}\kappa}{x^{\alpha_N} m_N})^{m_N}\right) \\ &\times (1 - e^{-\beta x}) x dx.\end{aligned} \tag{43}$$

In order to derive the expression for the SINR coverage probability in Theorem 2, we need to approximate the integral terms in (42) by closed-from expressions. To simplify the analysis, here we use the Gaussian-Chebyshev quadrature to find the closed-form expressions. As known, the Gaussian-Chebyshev quadrature can be expressed by [35, eq. (25.4.38)]

$$\int_{-1}^{1} f(x)(1-x^2)^{-1/2} dx = \frac{\pi}{K} \sum_{i=1}^{K} f(x_i) + \frac{\pi}{2^{2K-1}} \frac{f^{(2K)}(\xi)}{(2K)!} \tag{44}$$

for some $\xi \in [-1, 1]$, with quadrature nodes: $x_i = \cos(\frac{2i-1}{2K}\pi)$, $i = 1, \cdots, K$.

When employing the above approximation, we can replace variable x in (44) by $\frac{(\psi_u+1)R}{2}$, and then multiply the weight coefficient $(1-\psi_u)^{-1/2}$. Hence, $J_1(k)$ is approximated by

$$\begin{aligned}J_1(k) \approx &\frac{\pi R}{2U} \sum_{u=1}^{U} \sqrt{1-\theta_u^2} \psi_u e^{-\beta\psi_u} \\ &\times \left(1 - \left(1 + \frac{ra_L A_L \sum_{j=1}^{3} P_t Q_{j,k}\kappa}{\psi_u^{\alpha_L} m_L}\right)^{-m_L}\right).\end{aligned} \tag{45}$$

Similarly, we can obtain an approximated expression for $J_2(k)$ as

$$\begin{aligned}J_2(k) \approx &\frac{\pi R}{2U} \sum_{u=1}^{U} \sqrt{1-\theta_u^2} \psi_u (1 - e^{-\beta\psi_u}) \\ &\times \left(1 - \left(1 + \frac{ra_L A_L \sum_{j=1}^{3} P_t Q_{j,k}\kappa}{\psi_u^{\alpha_N} m_N}\right)^{-m_N}\right).\end{aligned} \tag{46}$$

By substituting (45), (46) into (41), a closed-form of $\Pr(\text{SINR} > T|\alpha_0 = \alpha_L)$ is obtained.

Given the desired link is NLOS, the conditional probability $\Pr(\text{SINR} > T|\alpha_0 = \alpha_N)$ can be derived similar to that for (41). Therefore, combining the above results with (11), and after some algebraic simplifications, we prove Theorem 2 straightforwardly.

Appendix C
Proof to Corollary 1

The SINR coverage probability of the typical SCBS can be evaluated by (11), which needs to derive the expressions for $\Pr(\text{SINR} > T|\alpha_0 = \alpha_L)$ and $\Pr(\text{SINR} > T|\alpha_0 = \alpha_N)$, conditioned on the desired link is either LOS or NLOS.

When considering Rayleigh fading scenario, we can apply the CDF of $F_Y(y) = 1 - e^{-y}$ (for Rayleigh distribution) to the derivation of the probabilities $\Pr(\text{SINR} > T|\alpha_0 = \alpha_L)$ and $\Pr(\text{SINR} > T|\alpha_0 = \alpha_N)$, and follow the approach similar to that in Appendix A. Then, upon employing the Gaussian-Chebyshev approximation used in Appendix B, the closed-form expressions for the probabilities can be obtained. In a

little more detail, the derivation for the probability $\Pr(\text{SINR} > T|\alpha_0 = \alpha_L)$ can be described as

$$\begin{aligned}
&\Pr(\text{SINR} > T|\alpha_0 = \alpha_L) \\
&= \int_0^\infty \left(|h_0|^2 > A_L(x+N_0)\right) f_{I_\Phi}(x)dx \\
&= e^{-a_L A_L N_0} E_{I_{\Phi_L}}\left[e^{-a_L A_L I_{\Phi_L}}\right] E_{I_{\Phi_N}}\left[e^{-a_L A_L I_{\Phi_N}}\right] \\
&= e^{-a_L A_L N_0} \\
&\quad \times \prod_{k=1}^{4} e^{-2\pi\lambda p_k \int_0^R \left(1-1/(1+\frac{a_L A_L \sum_{j=1}^3 P_t Q_{j,k}{}^\kappa}{x^{\alpha_L}})\right) e^{-\beta x} x dx} \\
&\quad \times \prod_{k=1}^{4} e^{-2\pi\lambda p_k \int_0^R \left(1-1/(1+\frac{a_L A_L \sum_{j=1}^3 P_t Q_{j,k}{}^\kappa}{x^{\alpha_N}})\right)(1-e^{-\beta x}) x dx} \\
&= e^{-a_L A_L N_0} \prod_{k=1}^{4} e^{-2\pi\lambda p_k (\tilde{J}_1(k)+\tilde{J}_2(k))}.
\end{aligned} \tag{47}$$

where $\tilde{J}_1(k)$ and $\tilde{J}_2(k)$ are expressed by (24) and (25). Similarly, the closed-form expression for the probability $\Pr(\text{SINR} > T|\alpha_0 = \alpha_N)$ can be given by

$$\begin{aligned}
&\Pr(\text{SINR} > T|\alpha_0 = \alpha_N) \\
&\quad = \int_0^\infty \Pr\left(|h_0|^2 > A_N(x+N_0)\right) f_{I_\Phi}(x)dx \\
&\quad = e^{-a_N A_N N_0} \prod_{k=1}^{4} e^{-2\pi\lambda p_k (\tilde{J}_3(k)+\tilde{J}_4(k))}.
\end{aligned} \tag{48}$$

where $\tilde{J}_3(k)$ and $\tilde{J}_4(k)$ can be found in (26) and (27). Finally, when substituting the results of (47) and (48) into (11) based on total probability theorem, Corollary 1 is proved.

Appendix D
Proof to Theorem 3

Using the SINR expression for the SBN model given by (29), the SINR coverage probability can be computed as

$$\begin{aligned}
P_c(T) &= \Pr\left(\kappa P_t D_0^{-\alpha_L}(G_0 - T\sum_{j=1}^{2} G_{0,j}) > T(I_{\Phi_L} + N_0)\right) \\
&\overset{(a)}{\approx} \Pr\left(\zeta > A_L(I_{\Phi_L} + N_0)\right) \\
&\overset{(b)}{\approx} 1 - E_{I_{\Phi_L}}\left[\left(1 - e^{-\eta A_L (I_{\Phi_L}+N_0)}\right)^N\right] \\
&= \sum_{v=1}^{V} \binom{V}{v} (-1)^{v+1} e^{-v\eta A_L N_0} E_{I_{\Phi_L}}\left[e^{-v\eta A_L I_{\Phi_L}}\right]
\end{aligned} \tag{49}$$

where $I_{\Phi_L} = \sum_{i>0, i\in\Phi_L} \sum_{j=1}^{3} P_t \tilde{G}_{i,j} \kappa D_i^{-\alpha_L}$ is the interference power observed by the typical SCBC. In (a), the dummy variable ζ is a normalized gamma variable with parameter V, and the approximation in (a) follows from the fact that a normalized Gamma distribution converges to identity when its parameter goes to infinity, i.e. $\lim_{v\to\infty} \frac{v^v x^{v-1} e^{-vx}}{\Gamma(v)} = \delta(x-1)$, where $\delta(x)$ is the Dirac delta function. The results in Theorem 3 generally provide a close approximation of $P_c(T)$ when enough terms are used, as this can be validated in remark 3.

Next, we focus on the computation of $E_{I_{\Phi_L}}\left[e^{-v\eta A_L I_{\Phi_L}}\right]$, given by

$$\begin{aligned}
&E_{I_{\Phi_L}}\left[e^{-v\eta A_L I_{\Phi_L}}\right] \\
&\overset{(c)}{=} e^{-\lambda \sum_{k=1}^{4} p_k \int_0^{2\pi}\int_0^{R_b} \left(1-e^{-\frac{v\eta A_L \sum_{j=1}^3 P_t Q_{j,k}{}^\kappa}{x^{\alpha_L}}}\right) x dx d\theta} \\
&= \prod_{k=1}^{4} e^{-2\pi\lambda p_k \int_0^{R_b} \left(1-e^{-\frac{v\eta A_L \sum_{j=1}^3 P_t Q_{j,k}{}^\kappa}{x^{\alpha_L}}}\right) x dx} \\
&\overset{(d)}{\approx} \prod_{k=1}^{4} e^{-2\pi\lambda p_k \hat{J}(k)}
\end{aligned} \tag{50}$$

where step (c) is due to computing the Laplace functional of the PPP I_{Φ_L}, and step (d) is obtained by applying the Gaussian-Chebyshev quadrature, and similar derivation procedures can be found in Appendix B. In addition, $\hat{J}(k)$ is given by

$$\hat{J}(k) = \frac{\pi R_b}{2W} \sum_{w=1}^{W} \sqrt{1-\theta_w^2}\, \psi_w \left(1 - e^{-\frac{v\eta A_L \sum_{j=1}^3 P_t Q_{j,k}{}^\kappa}{\psi_w^{\alpha_L}}}\right) \tag{51}$$

where $\theta_w = \cos(\frac{2w-1}{2W}\pi)$, $\psi_w = \frac{(\theta_w+1)R_b}{2}$, and W denotes an accuracy-complexity trade-off parameter. Combining (51) with (50), Theorem 3 is proved straightforwardly.

Appendix E
Proof to Lemma 2

According to the analysis in Section III, we can summarize the expressions for the SINR coverage probabilities of the SBN model, and rewrite the ASE as

$$\begin{aligned}
\eta_{ASE}(P_{t,n}) &= \hat{\lambda}\hat{N}\log_2(1+T) \\
&\quad \times \left[\sum_{r=1}^{Z} X_r e^{-\frac{\varphi_r}{P_{t,n}(G_0 - T\sum_{j=1}^2 G_{0,j})}}\right]
\end{aligned} \tag{52}$$

where the expressions for φ_r, X_r, Θ_r can be easily known from (30) in Theorems 3. To guarantee the problem of $\mathcal{P}_1$ concave, it needs to prove that the objective function and the inequality constraint functions are all concave.

Let us now prove that the objective function $F(q_n, P_{t,n})$ of problem $\mathcal{P}_1$ is concave. Note that, we can rewrite the objective function as $F(q_n, P_{t,n}) = F_1 - F_2$, where F_2 is linear function known from (36). Hence, we only need to prove that F_1 is concave. After some calculations, the second derivative of F_1 can be given by

$$\begin{aligned}
\frac{\mathrm{d}^2 F_1}{\mathrm{d}P_{t,n}^2} &= \frac{\hat{\lambda}\hat{N}\log_2(1+T)}{P_{t,n}^4 (G_0 - T\sum_{j=1}^2 G_{0,j})^2} \\
&\quad \times \sum_{r=1}^{Z} X_r \phi_r e^{-\frac{\varphi_r}{P_{t,n}(G_0 - T\sum_{j=1}^2 G_{0,j})}} \\
&\quad \times \left[\phi_r - 2P_{t,i}(G_0 - T\sum_{j=1}^{2} G_{0,j})\right] \\
&= \frac{\hat{\lambda}\hat{N}\log_2(1+T)}{P_{t,n}^4 (G_0 - T\sum_{j=1}^2 G_{0,j})^2} \sum_{r=1}^{Z} \hat{f}(r)\ .
\end{aligned} \tag{53}$$

It readily finds the first fraction part in (53) is non-negative. We find that $\hat{f}(r=1) < 0 \,\&\, \hat{f}(r=1) << \hat{f}(r \geq 1), \forall r \leq Z$, when applying the parameters in Section VI to function $\hat{f}(r)$. Hence, the second derivative of F_1 is non-positive and hence, the objective function $F(q_i, P_{t,i})$ is concave.

Similarly, when substituting (52) into the constraint of (33), we derive the expressions for the constraint, which is concave. In addition, constraint (34) is a linear function. Hence, the optimization problem in $\mathcal{P}_0$ is a concave problem. Furthermore, the objective function $F(q_i, P_{t,i})$ for problem $\mathcal{P}_1$ will converge to 0, and the proof for this convergence is in [39].

REFERENCES

[1] R. Q. Hu and Y. Qian, "An energy efficient and spectrum efficient wireless heterogeneous network framework for 5G systems," *IEEE Commun. Mag.*, vol. 52, no. 5, pp. 94–101, May 2014.

[2] X. Ge, S. Tu, G. Mao, and C. X. Wang, "5G ultra-dense cellular networks," *IEEE Trans. Wireless Commun.*, vol. 23, no. 1, pp. 72–79, Feb. 2016.

[3] X. Ge, S. Tu, T. Han, and Q. Li, "Energy efficiency of small cell backhaul networks based on Gauss–Markov mobile models," *IET Netw.*, vol. 4, no. 2, pp. 158–167, 2015.

[4] X. Gao, L. Dai, S. Han, I. Chih-Lin, and R. W. Heath, Jr., "Energy-efficient hybrid analog and digital precoding for mmWave MIMO systems with large antenna arrays," *IEEE J. Sel. Areas Commun.*, vol. 34, no. 4, pp. 998–1009, Apr. 2016.

[5] L. Li, Y. Xu, Z. Zhang, J. Yin, W. Chen, and Z. Han, "A prediction-based charging policy and interference mitigation approach in the wireless powered Internet of Things," *IEEE J. Sel. Areas Commun.*, vol. 37, no. 3, pp. 1–13, 2018.

[6] X. Gao, L. Dai, C. Yuen, and Z. Wang, "Turbo-like beamforming based on tabu search algorithm for millimeter-wave massive MIMO systems," *IEEE Trans. Veh. Technol.*, vol. 65, no. 7, pp. 5731–5737, Jul. 2016.

[7] Y. Hao, Q. Ni, H. Li, and S. Hou, "On the energy and spectral efficiency tradeoff in massive MIMO-enabled HetNets with capacity-constrained backhaul links," *IEEE Trans. Commun.*, vol. 65, no. 11, pp. 4720–4733, Nov. 2017.

[8] C. Yang, J. Li, Q. Ni, A. Anpalagan, and M. Guizani, "Interference-aware energy efficiency maximization in 5G ultra-dense networks," *IEEE Trans. Commun.*, vol. 65, no. 2, pp. 728–739, Feb. 2017.

[9] T. S. Rappaport *et al.*, "Millimeter wave mobile communications for 5G cellular: It will work!" *IEEE Access*, vol. 1, pp. 335–349, May 2013.

[10] S. Rangan, T. S. Rappaport, and E. Erkip, "Millimeter-wave cellular wireless networks: Potentials and challenges," *Proc. IEEE*, vol. 102, no. 3, pp. 366–385, Mar. 2014.

[11] T. Bai and R. W. Heath, Jr., "Coverage and rate analysis for millimeter-wave cellular networks," *IEEE Trans. Wireless Commun.*, vol. 14, no. 2, pp. 1100–1114, Feb. 2015.

[12] C. Wang and H.-M. Wang, "Physical layer security in millimeter wave cellular networks," *IEEE Trans. Wireless Commun.*, vol. 15, no. 8, pp. 5569–5585, Aug. 2016.

[13] Y. Ju, H. M. Wang, T. X. Zheng, and Q. Yin, "Secure transmissions in millimeter wave systems," *IEEE Trans. Commun.*, vol. 65, no. 5, pp. 2114–2127, May 2017.

[14] R. Taori and A. Sridharan, "Point-to-multipoint in-band mmWave backhaul for 5G networks," *IEEE Commun. Mag.*, vol. 53, no. 1, pp. 195–201, Jan. 2015.

[15] W. Kim, "Dual connectivity in heterogeneous small cell networks with mmWave backhauls," *Mobile Inf. Syst.*, vol. 2016, Sep. 2016, Art. no. 3983467.

[16] J. Park, S.-L. Kim, and J. Zander, "Tractable resource management with uplink decoupled millimeter-wave overlay in ultra-dense cellular networks," *IEEE Trans. Wireless Commun.*, vol. 15, no. 6, pp. 4362–4379, Jun. 2016.

[17] J. Park, S.-L. Kim, and J. Zander, "Resource management and cell planning in millimeter-wave overlaid ultra-dense cellular networks," in *Proc. 12th IEEE VTS Asia–Pacific Wireless Commun. Symp. (APWCS)*, Singapore, Aug. 2015, pp. 1–6.

[18] D. Li, W. Saad, and C. S. Hong, "Decentralized renewable energy pricing and allocation for millimeter wave cellular backhaul," *IEEE J. Sel. Areas Commun.*, vol. 34, no. 5, pp. 1140–1159, May 2016.

[19] M. N. Islam, A. Sampath, A. Maharshi, O. Koymen, and N. B. Mandayam, "Wireless backhaul node placement for small cell networks," in *Proc. Annu. Conf. Inf. Sci. Syst.*, Mar. 2014, pp. 1–6.

[20] X. Xu, W. Saad, X. Zhang, X. Xu, and S. Zhou, "Joint deployment of small cells and wireless backhaul links in next-generation networks," *IEEE Commun. Lett.*, vol. 19, no. 12, pp. 2250–2253, Dec. 2015.

[21] M. Shariat, E. Pateromichelakis, A. ul Quddus, and R. Tafazolli, "Joint TDD backhaul and access optimization in dense small-cell networks," *IEEE Trans. Vehicle Technol.*, vol. 64, no. 11, pp. 5288–5299, Nov. 2015.

[22] S. T. Choi, K. S. Yang, S. Nishi, S. Shimizu, K. Tokuda, and Y. H. Kim, "A 60-GHz point-to-multipoint millimeter-wave fiber-radio communication system," *IEEE Trans. Microw. Theory Techn.*, vol. 54, no. 5, pp. 1953–1960, May 2006.

[23] Y. Nagai, M. Ochiai, A. Taira, T. Yamauchi, N. Shimizu, and A. Shibuya, "On the design of a point-to-multipoint gigabit WLAN system on 60 GHz millimeter wave," in *Proc. IEEE Consum. Commun. Netw. Conf.*, Jan. 2009, pp. 1–5.

[24] P. Wang, Y. Li, L. Song, and B. Vucetic, "Multi-gigabit millimeter wave wireless communications for 5G: From fixed access to cellular networks," *IEEE Commun. Mag.*, vol. 53, no. 1, pp. 168–178, Jan. 2015.

[25] J. A. Zhang *et al.*, "Low latency integrated point-to-multipoint and E-band point-to-point backhaul for mobile small cells," in *Proc. IEEE Int. Conf. Commun. Workshops (ICC)*, Jun. 2014, pp. 592–597.

[26] R. Vilar, J. Martí, and F. Magne, "Point to multipoint wireless backhaul systems for cost-effective small cell deployment," in *Proc. Eur. Microw. Conf. (EuMC)*, Sep. 2015, pp. 1092–1095.

[27] F. André *et al.*, "Fabrication of W-band TWT for 5G small cells backhaul," in *Proc. Int. Vac. Electron. Conf.*, Apr. 2017, pp. 1–2.

[28] C. Paoloni *et al.*, "Tweether future generation W-band backhaul and access network infrastructure and technology," in *Proc. IEEE EUCNC*, Oulu, Finland, Jun. 2017, pp. 1–5.

[29] M. N. Kulkarni, J. G. Andrews, and A. Ghosh, "Performance of dynamic and static TDD in self-backhauled millimeter wave cellular networks," *IEEE Trans. Wireless Commun.*, vol. 16, no. 10, pp. 6460–6478, Oct. 2017.

[30] J. G. Andrews, T. Bai, M. N. Kulkarni, A. Alkhateeb, A. K. Gupta, and R. W. Heath, Jr., "Modeling and analyzing millimeter wave cellular systems," *IEEE Trans. Commun.*, vol. 65, no. 1, pp. 403–430, Jan. 2017.

[31] M. Haenggi, *Stochastic Geometry for Wireless Networks*. Cambridge, U.K.: Cambridge Univ. Press, 2012.

[32] J. G. Andrews, R. K. Ganti, M. Haenggi, N. Jindal, and S. Weber, "A primer on spatial modeling and analysis in wireless networks," *IEEE Commun. Mag.*, vol. 48, no. 11, pp. 156–163, Nov. 2010.

[33] A. Goldsmith, *Wireless Communications*. Cambridge, U.K.: Cambridge Univ. Press, 2005.

[34] R. Hernandez-Aquino, S. A. R. Zaidi, D. McLernon, M. Ghogho, and A. Imran, "Tilt angle optimization in two-tier cellular networks—A stochastic geometry approach," *IEEE Trans. Commun.*, vol. 63, no. 12, pp. 5162–5177, Dec. 2015.

[35] M. Abramowitz and I. Stegun, *Handbook of Mathematical Functions: With Formulas, Graphs, and Mathematical Tables*. New York, NY, USA: Dover, 1972.

[36] F. B. Hildebrand, *Introduction to Numerical Analysis*. New York, NY, USA: Dover, 1987.

[37] G. Lee, Y. Sung, and J. Seo, "Randomly-directional beamforming in millimeter-wave multiuser MISO downlink," *IEEE Trans. Wireless Commun.*, vol. 15, no. 2, pp. 1086–1100, Feb. 2016.

[38] T. S. Rappaport, E. Ben-Dor, J. N. Murdock, and Y. Qiao, "38 GHz and 60 GHz angle-dependent propagation for cellular & peer-to-peer wireless communications," in *Proc. Int. Conf. Commun. (ICC)*, Ottawa, ON, Canada, Jun. 2012, pp. 4568–4573.

[39] W. Dinkelbach, "On nonlinear fractional programming," *Manage. Sci.*, vol. 13, no. 7, pp. 492–498, Mar. 1967.

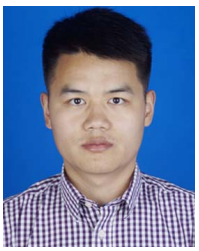

Jia Shi received the M.Sc. and Ph.D. degrees from the University of Southampton, U.K., in 2010 and 2015, respectively. He was a Research Associate with Lancaster University, U.K., from 2015 to 2017. He was a Research Fellow with 5GIC, University of Surrey, U.K., from 2017 to 2018. Since 2018, he has been with Xidian University, China, where he is currently an Associate Professor with the State Key Laboratory of Integrated Services Networks. His current research interests include mm-wave communications, artificial intelligence, resource allocation in wireless systems, covert communications, physical layer security, and cooperative communication.

Lu Lv received the Ph.D. degree in communication and information systems from Xidian University, China, in 2018. In 2016, he was a Visiting Ph.D. Student with the School of Computing and Communications, Lancaster University, U.K. From 2016 to 2018, he was a Visiting Ph.D. Student with the Department of Electrical and Computer Engineering, University of Alberta, Canada. He is currently a Research Fellow with the State Key Laboratory of Integrated Services Networks, Xidian University. His research interests include cooperative communications, non-orthogonal multiple access, physical layer security, and mm-wave communications.

Qiang Ni (M'04–SM'08) received the B.Sc., M.Sc., and Ph.D. degrees from the Huazhong University of Science and Technology, China, all in engineering. He is currently a Professor and the Head of the Communication Systems Group, School of Computing and Communications, Lancaster University, Lancaster, U.K. His research interests include the areas of future generation communications and networking, including green communications and networking, mm-wave wireless communications, cognitive radio network systems, non-orthogonal multiple access, heterogeneous networks, 5G and 6G, SDN, cloud networks, energy harvesting, wireless information and power transfer, IoTs, cyber physical systems, machine learning, big data analytics, and vehicular networks. He has authored or co-authored over 200 papers in these areas. He was an IEEE 802.11 Wireless Standard Working Group Voting Member and a contributor to the IEEE Wireless Standards.

Haris Pervaiz (S'09–M'09) received the M.Sc. degree in information security from the Royal Holloway University of London, Egham, U.K., in 2005, and the Ph.D. degree from the School of Computing and Communication, Lancaster University, Lancaster, U.K., in 2016. From 2017 to 2018, he was a Research Fellow with the 5G Innovation Centre, University of Surrey, Guildford, U.K. From 2016 to 2017, he was an EPSRC Doctoral Prize Fellow with the School of Computing and Communication, Lancaster University. He is currently an Assistant Professor (Lecturer) with the School of Computing and Communications, Lancaster University. His current research interests include green heterogeneous wireless communications and networking, 5G and beyond, mm-wave communication, and energy and spectral efficiency. He is an Associate Editor of the IEEE ACCESS and *Internet Technology Letters* (Wiley), and is on the Editorial Board of the *Emerging Transactions on Telecommunications Technologies* (Wiley).

Claudio Paoloni (M'86–SM'11) received the degree *(cum laude)* in electronic engineering from the Sapienza University of Rome, Rome, Italy, in 1984. Since 2012, he has been a Professor of electronics with the Department of Engineering, Lancaster University, Lancaster, U.K. Since 2015, he has been the Head of the Engineering Department. He is a Coordinator of the European Commission Horizon 2020 Project TWEETHER "Traveling Wave Tube-Based W-Band Wireless Network for High Data Rate, Distribution, Spectrum and Energy Efficiency" and of the Horizon 2020 ULTRAWAVE Project "Ultra-Capacity Wireless Layer Beyond 100 GHz Based on Millimeter Wave Traveling Wave Tubes" for millimeter waves high capacity wireless networks. He has authored more than 200 publications. His research focuses on microwave and millimeter wave technologies for vacuum electronics and wireless communications. He is the Chair of the IEEE Electron Device Society Vacuum Electronics Technical Committee.